[American Journal of Science, Vol. 313, December, 2013, P. 1017–1053, DOI 10.2475/10.2013.03]

TELESCOPING METAMORPHIC ISOGRADS: EVIDENCE FROM $^{40}Ar/^{39}Ar$ DATING IN THE ORANGE-MILFORD BELT, SOUTHERN CONNECTICUT

MARTHA L. GROWDON*,†, MICHAEL J. KUNK**, ROBERT P. WINTSCH***, and GREGORY J. WALSH§

ABSTRACT. New $^{40}Ar/^{39}Ar$ ages for hornblende and muscovite from the Orange-Milford belt in southern Connecticut reflect cooling from Acadian amphibolite facies metamorphism between ~380 to 360 Ma followed by retrograde recrystallization of fabric-forming muscovite and chlorite during lower greenschist facies Alleghanian transpression at ~280 Ma. Reported field temperature and pressure gradients are improbably high for these rocks and a NW metamorphic field gradient climbing from chlorite-grade to staurolite-grade occurs over less than 5 km. Simple tilting cannot account for this compressed isograd spacing given the geothermal gradient of ~20 °C/km present at the time of regional metamorphism. However, post-metamorphic transpression could effectively telescope the isograds by stretching the belt at an oblique angle to the isograd traces. Textures in the field and in thin section reveal several older prograde schistosities overprinted by lower greenschist facies fabrics. The late cleavages commonly occur at the scale of ~100 μm and these samples contain multiple age populations of white mica. $^{40}Ar/^{39}Ar$ analysis of these poly-metamorphic samples with mixed muscovite populations yield climbing or U-shaped age spectra. The ages of the low temperature steps are late Paleozoic, while the ages of the older steps are late Devonian. These results support our petrologic interpretation that the younger cleavage developed under metamorphic conditions below the closure temperature for Ar diffusion in muscovite, that is, in the lower greenschist facies. The correlation of a younger regionally reproducible age population with a pervasive retrograde muscovite ± chlorite cleavage reveals an Alleghanian (~280 Ma) overprint on the Acadian metamorphic gradient (~380 Ma). Outcrop-scale structures including drag folds and imbricate boudins suggest that Alleghanian deformation and cleavage development occurred in response to dextral transpression along a northeast striking boundary. Alleghanian oblique collision of accreting terranes from the northeast would have resulted in northeast-southwest dextral transpression against the New York promontory. This deformation was responsible for crystallization of pervasive retrograde muscovite + chlorite cleavages and associated telescoping of the Acadian metamorphic isograds in southern Connecticut at ~280 Ma.

Key words: Alleghanian overprint, compressed isograds, polymetamorphism, $^{40}Ar/^{39}Ar$ thermochronology

INTRODUCTION

Compressed isograds are a common occurrence in metamorphic terranes where regional extensional strain has occurred (for example, Passchier, 1984). This extension must occur after peak metamorphic temperatures because thermal relaxation during sustained prograde metamorphism would reestablish regional geothermal gradients and produce "normal" metamorphic field gradients. The inverted isograds of the Himalayas are well known for telescoping where isograds are not only compressed but also inverted in the hanging wall of the Main Central Thrust (for example,

* Department of Earth and Atmospheric Sciences, SUNY Oneonta, 209 Science Building 1, Oneonta, New York 13820
** US Geological Survey, 12201 Sunrise Valley Drive, Reston, Virginia 20192
*** Department of Geological Sciences, Indiana University, 1001 East 10th Street, Bloomington, Indiana 47405
§ US Geological Survey, 87 State Street, Montpelier, Vermont 05602
† Corresponding author: martha.growdon@gmail.com

Mukherjee and Koyi, 2010; Streule and others, 2010). Isograds in core complexes and gneiss dome settings (Crittenden, 1980; Passchier, 1984; Olivier and others, 2004) and transpressive regimes (Phillips and Auton, 1997) may also be compressed. In some cases, metamorphic convergence of the hanging and foot walls can occur (Jacobson, 1997).

Mylonites and phyllonites formed in ductile fault zones are commonly involved in thinning isograds where these fault zones juxtapose high grade terranes (Sturt and others, 1978). Strain can be localized in mylonitic rocks in which retrograde reactions producing phyllosilicates and quartz are penetrative and weaken these rocks; such mylonites can occur in belts wide enough to be mappable (Boronkay and Doutsos, 1994). Terranes with more widely distributed retrograde fabrics in which strain is pervasive, not localized, are not as well described in the literature but can be recognized by overprinting fabrics (for example, Ratcliffe, 1994). Perhaps the reason for this is the lack of strain markers and clearly definable fault zones. Still, such rocks have been described as diaphthorites or diaphthoritic gneisses, especially in Europe and have been known for over 100 years (for example, Heritsch, 1912; Hsu, 1955).

At the outcrop scale retrograde overprinting may be structural or metamorphic or both. Refolded folds commonly preserve geometric evidence for multiple deformation events, even in high grade rocks. However, mineralogical evidence of earlier metamorphic events is less well preserved because the heat added in prograde metamorphism provides the activation energy to recrystallize and thereby destroy earlier metamorphic minerals. Both strain and fluid infiltration can also provide the activation energy for recrystallization in high grade rocks and together are probably responsible for the retrograde fabrics that occur in transpressive fault zones.

In this contribution we examine rocks in which a collapsed metamorphic field gradient was mapped at the quadrangle scale (Fritts, 1962, 1965a, 1965b), and the steepness of this gradient later quantified (Ague, 2002, 2005). The Orange-Milford belt (OMB) of greenschist to amphibolite facies rocks lies between still higher-grade peri-Laurentian terranes to the west and peri-Gondwanan terranes to the east, but this curious tectonic setting has been largely unexplored. Here we build on the work of Ague by investigating fabrics and using $^{40}Ar/^{39}Ar$ thermochronology of amphibole and muscovite to test the hypotheses that 1) the primary metamorphism in the OMB was indeed Acadian and 2) that this belt has indeed been thinned, by as much as a factor of two, by a late Paleozoic, transpressive, diaphthoritic event. We close by exploring the large-scale tectonic movements that might have been responsible for this event.

GEOLOGIC SETTING

Lithotectonic terranes in the southwestern corner of New England are characterized by polydeformed, polymetamorphosed rocks. They are cored by Mesoproterozoic Grenvillian gneisses exposed in the west (for example, Rodgers, 1985) as part of the Laurentian basement and its early Paleozoic sedimentary cover. Cambrian and Ordovician peri-Laurentian shelf/slope sediments and arc-related rocks of the Rowe-Hawley zone lie to the east of this basement. They were accreted to Laurentia by thrust faults that imbricated cover rocks with slices of Grenville basement gneisses (Ratcliffe and Bahrami, 1976) and metamorphosed during the high-grade Ordovician Taconic orogeny (Hibbard and others, 2006). This modified Laurentian margin was unconformably overlain by younger Silurian and Devonian metasedimentary rocks of the Connecticut Valley Synclinorium (Hibbard and others, 2006). East of New York, all of these rocks were variably overprinted by the Early Devonian Acadian orogeny (for example, Wintsch and others, 1992; Sevigny and Hanson, 1993; Ague, 1994b; Hibbard and others, 2006; Lancaster and others, 2008; Dietsch and others, 2010). The thermal effects of the subsequent Alleghanian orogeny are documented primarily in Permian cooling ages of micas in southwestern Connecticut (Moecher and others, 1997).

The Orange-Milford belt contains a northeast-striking sequence of metasedimentary rocks on the southeastern margin of Connecticut's accreted Rowe-Hawley zone. The OMB contains the Silurian to Devonian Wepawaug Schist, and the Ordovician Oronoque Schists and Maltby Lakes and Allingtown Metavolcanics (Rodgers, 1985). It is unconformably overlain on the east by Triassic arkoses of the New Haven Formation in the Hartford basin. The Wepawaug Schist projects northeast under this basin and has been correlated to the lithologically similar Waits River and Northfield Formations in Massachusetts and Vermont (for example, Fritts, 1962; Goldsmith and others, 1983; Bell and Newman, 2006; McWilliams, ms, 2008).

The western margin of the OMB is much more complicated. It is marked by a band of diaphthoritic schists facing a Silurian orthogneiss called the Pumpkin Ground Gneiss (Sevigny and Hanson, 1993). Between this orthogneiss and the Wepawaug Schist, Fritts (1965a) maps four lenses of schistose and phyllitic rocks as stratigraphic units, while recognizing their retrograde character. Rodgers (1985) assigns three of these units to the Silurian-Devonian Straits Schist, and separates them from the Wepawaug Schist by the East Derby Fault. One of Fritts' (1965a) units is the highly sheared Derby Hill Schist (Odo), a 300-meter wide band of schist and phyllite stretching 20 km along the western margin of the Wepawaug Schist. In reconnaissance conducted for this study the Derby Hill Schist was found to contain multiple generations of crenulated cleavages preserved in microlithons and tectonic inclusions bounded by phyllonites. These rocks are sandwiched between Kyanite grade rocks of the Pumpkin Ground Gneiss and the Wepawaug schist. With this evidence, we refer to this zone as the East Derby shear zone (EDSZ, fig. 1), recognizing that it is a mappable band of diaphthoritic fault rocks.

Fritts (1965a) also mapped a regional-scale syncline, the Wepawaug Syncline, as the dominant structural feature between the Straits Schist and the Triassic unconformity. This was based in part on stratigraphic correlation of mafic schists east of the Wepawaug Schist with amphibolites to the west. However, petrographic observations made here suggest the amphibolite mapped west of the Wepawaug Schist is intercalated with argillaceous schist and that mapped east of the Wepawaug Schist is distinct metavolcanic rock, part of the Maltby Lakes Metavolcanics. Further work is needed to explore whether the Maltby Lakes volcanic sequence convincingly occurs west of the Wepawaug Schist to corroborate Fritts' (1965a) stratigraphic correlation.

Most of the OMB is occupied by the Wepawaug Schist and contains a typical Barrovian-style metamorphic gradient. It is defined by well-developed porphyroblasts of biotite, garnet, staurolite, and kyanite in a schistose matrix of phyllosilicate minerals (Fritts, 1965a; Ague, 1994b, 2002). Metamorphic grade decreases east of the EDSZ over a distance of ~4-km from staurolite/kyanite- to chlorite-grade. Thermobarometry in these rocks shows a decrease of 200 °C and 4 kbar (Ague, 2002) along this transect reflecting a syn-metamorphic geothermal gradient of *ca.* 19 °C/km. This geothermal gradient requires a vertical separation of ~8 km between the biotite/garnet and staurolite/kyanite isograds during peak metamorphism. However, the present metamorphic field gradient is ~50 °C/km and 50 MPa/km. This steep geothermal gradient is inconsistent with the kyanite grade metamorphism, while the geobaric gradient is unattainable given the density of normal crustal rocks. Geochronology in the U-Pb system suggests that this high-grade metamorphism occurred during the Middle Devonian (Sevigny and Hanson, 1993; Lanzirotti and Hanson, 1996; Lancaster and others, 2008), but the possibility of an Alleghanian thermal or dynamic overprint has not been explored. The present research was designed to explore the possibility of an Alleghanian overprint using $^{40}Ar/^{39}Ar$ thermochronology of amphibole and musco-

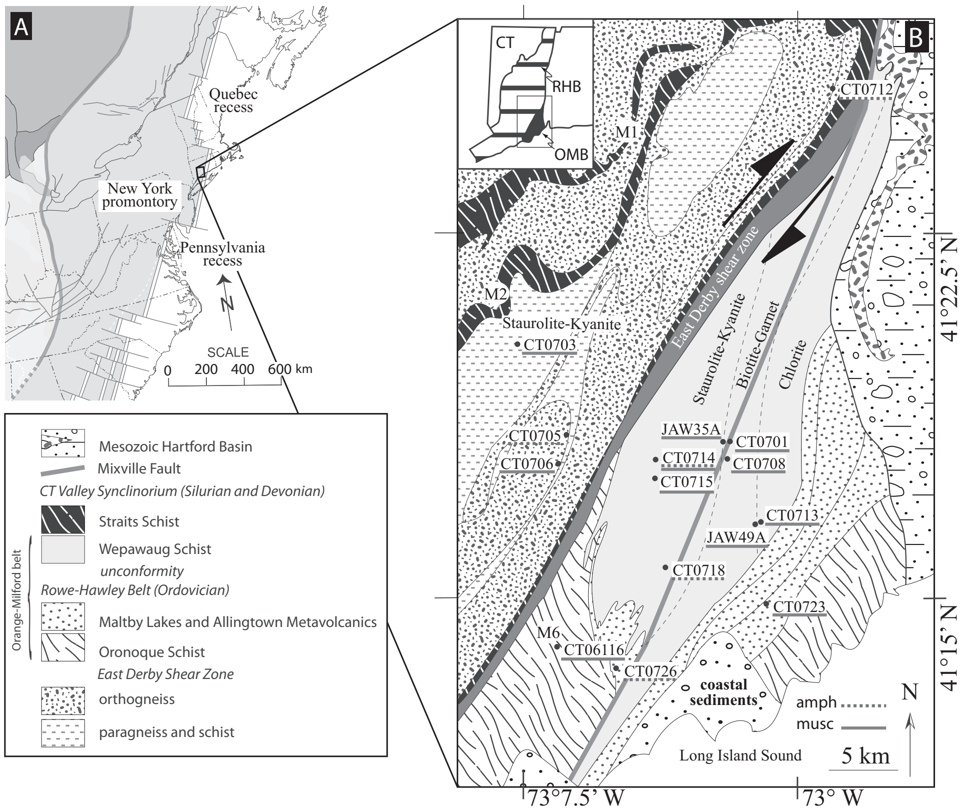

Fig. 1. (A) Generalized tectonic map of Grenville basement boundary (gray double dotted line) during the opening of the Iapetus Ocean showing promontories and recesses along the east coast of North America (modified after Thomas, 2006). (B) Generalized geologic map of the study area (modified after Ague, 1994a, 2002) with isograds and argon sample locations identified (table 3). The location of the OMB relative to the Rowe-Hawley Belt in southern Connecticut is shown in the inset. M1, M2, M6 refer to sample locations of Moecher, Cosca, and Hanson (1997).

vite and to investigate the causes of the unusual metamorphic field gradient identified and quantified by Ague (2002).

Methods

Microprobe Analysis

Biotite, muscovite, and chlorite grains were quantitatively analyzed using wavelength-dispersive analysis with the CAMECA SX-50 electron microprobe at Indiana University. A 20 nA beam current and 15 kV accelerating voltage were used to analyze phyllosilicate chemistries in 3 μm circular spots. Of the elements important to this study, analytical errors from counting statistics varied from 0.5 percent relative for high-concentration elements (for example, SiO_2) to 6 percent relative for low-concentration elements (for example, TiO_2). The reproducibility of analyses from single grains suggests that these error estimates are maximum values.

$^{40}Ar/^{39}Ar$ Methods

High-purity (>99%) mineral separates were analyzed using the $^{40}Ar/^{39}Ar$ age-spectrum-dating technique. Rock samples were crushed, ground, sieved, and minerals were concentrated using standard magnetic and density separation techniques. Ultrasonic abrading and cleaning of mineral concentrates was followed by additional magnetic and density separation and handpicking. Every effort was made to separate chlorite and epidote from muscovite and amphibole separates, respectively, but in some samples the minerals were so intergrown that complete separation was not achieved. Aliquots of muscovite (~10 mg) and amphibole (~100 mg) were packaged in copper and irradiated at the U.S. Geological Survey TRIGA reactor (Dalrymple and others, 1981). Standard MMhb-1 with an age of 519.4 Ma (Alexander and others, 1978; Dalrymple and others, 1981) was used as the fluence monitor. The samples were then incrementally heated in a low-blank furnace for ten minutes per step. After removing impurities, each heating step was analyzed in a VG MM 1200b mass spectrometer, operated in the static mode. Data reduction was accomplished using an updated version of ArAr* (Haugerud and Kunk, 1988) and the decay constants recommended by Steiger and Jäger (1977). Plateau ages, when they occur, are defined using the criteria of Fleck and others (1977) as modified by Haugerud and Kunk (1988) which state that 50 percent or more of the ^{39}Ar from the age spectrum must be released in two or more contiguous steps that agree in age within the limits of analytical precision.

Inverse isochrons were calculated for amphibole samples using the method of York (1969). Meaningful inverse isochron ages, for this study, contain 45 percent or more of the ^{39}Ar released from the sample, have a mean square of weighted deviates (MSWD) of ≤ 2.5, a calculated initial $^{40}Ar/^{36}Ar$ ratio of ≥ 295.5, and are equal to or younger than the minimum acceptable age step in the spectrum within the limits of analytical precision. If these criteria were not met, individual points were deleted from the low- and/or high-temperature portion of the analysis to improve the fit. Several of the inverse isochrons from the amphibole samples did not yield meaningful results but are presented for completeness. Inverse isochron analysis is not appropriate, and thus is not presented, for the muscovite separates because they contain mixtures of white micas of different ages.

RESULTS

Following petrographic examination of >100 samples, 15 samples with mineral assemblages and textures appropriate for this investigation were selected for muscovite and amphibole $^{40}Ar/^{39}Ar$ thermochronology (fig. 1B) to document the regional post-peak metamorphic evolution. Detailed electron petrography and microprobe analyses of five representative samples from across the metamorphic gradient in the Wepawaug Schist are described below.

Structures

Rocks of the OMB are highly folded at the meter-scale and are characterized by multiple crosscutting sub-parallel cleavages and folded and/or boudinaged quartz veins that are sub-parallel to the cleavages (fig. 2). Most schistose samples contain well-developed crenulation cleavages. The discussion of these fabrics below follows the terminology of Gray (1977) who describes crenulation cleavages as having domains of aligned phyllosilicates (P-domains) that cut older fabrics (microlithons). Where the microlithons contain abundant quartz and feldspar relative to the P-domains they are called QF-domains. Crenulation cleavage morphology is divided into two types: zonal crenulation cleavages have gradational boundaries between cleavage domains, whereas discrete crenulation cleavages have abruptly truncated boundaries (Gray, 1977; McWilliams and others, 2007). Both types of cleavages are found in these rocks (fig. 3). To simplify discussion and interpretation of the results, we anticipate the conclusion that the truncating chlorite + muscovite fabrics are Alleghanian in age so we describe them in textures with the symbol S(al) (for example, fig. 3A). We also anticipate that fabrics truncated by this Alleghanian chlorite + muscovite fabric grew during the Acadian

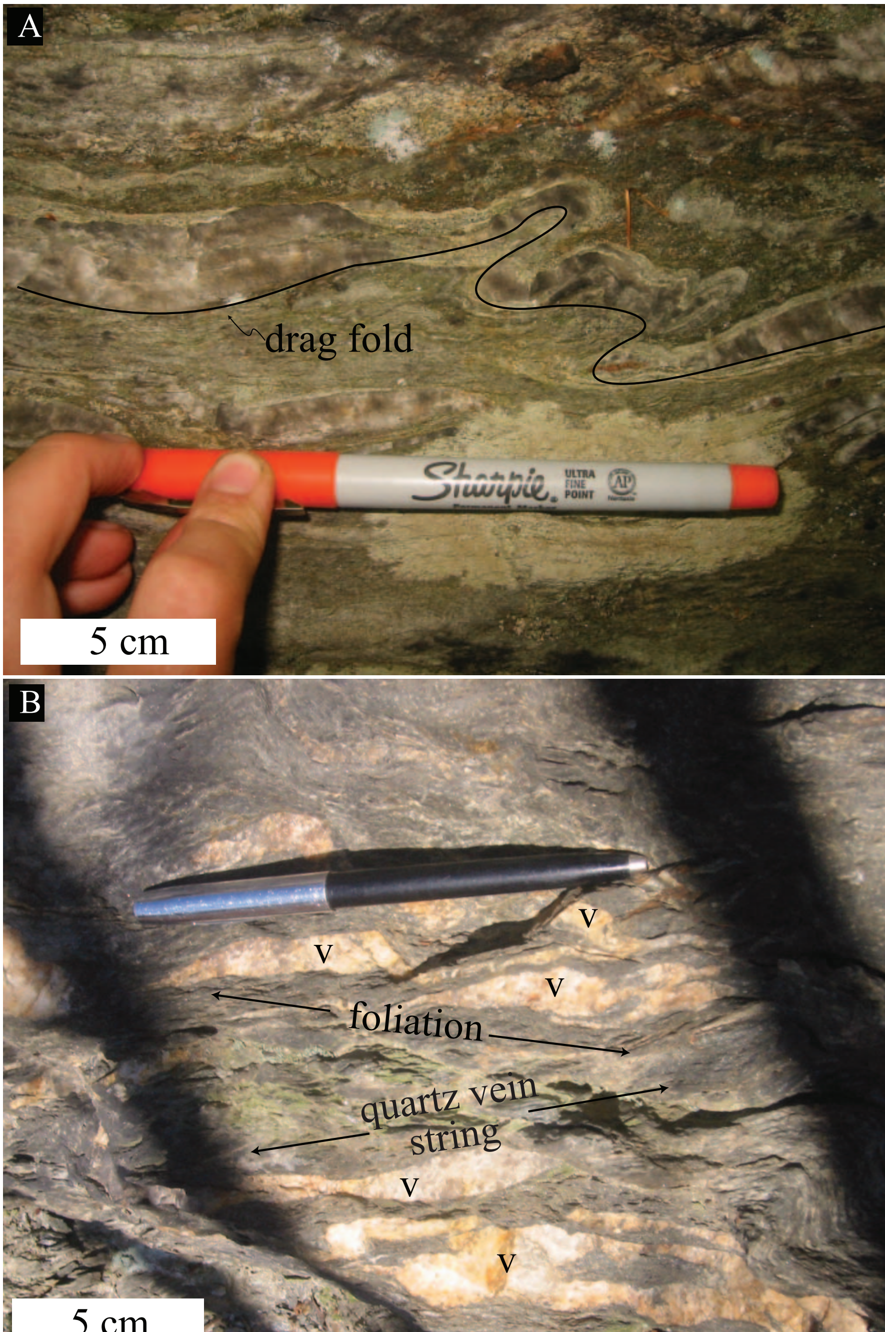

Fig. 2. Outcrop images of typical schists from the OMB showing (A) a drag fold with dextral offset (location 41°20′43.5″ N, 73°3′18.9″ W), (B) strings of dextrally sheared quartz veins climbing up and cutting a foliation (location 41°17′33.93″ N, 73° 5′5.12″ W). All coordinates reported in WGS84 horizontal datum.

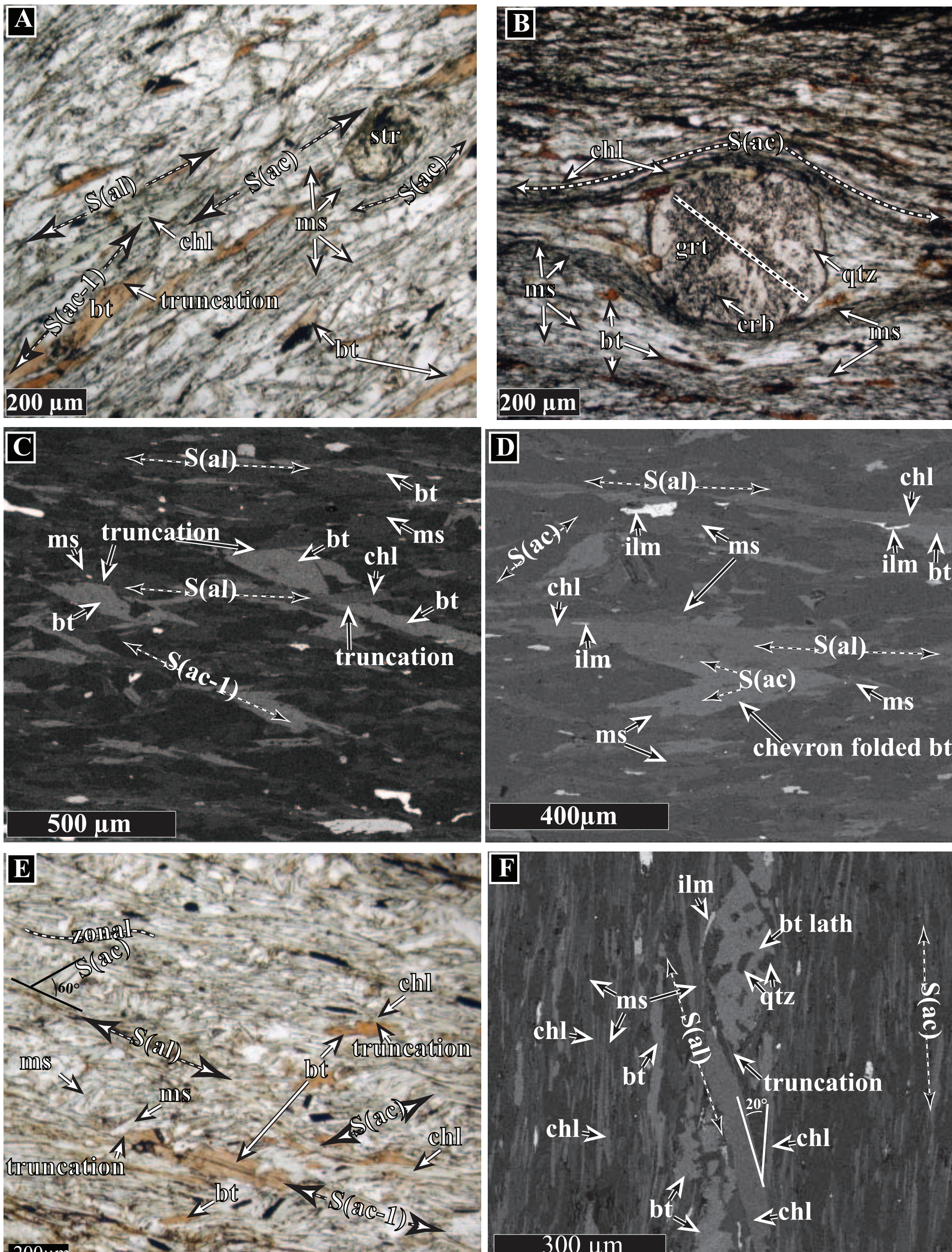

Fig. 3. Plane polarized light and backscattered electron (BSE) images showing typical mineral assemblages, fabrics, and textures in staurolite-, biotite-, and chlorite-grade schists and phyllites from the OMB. (A, B) Plane polarized light photomicrographs of staurolite schist with garnet and staurolite porphyroblasts. Dashed white line in garnet indicates trace of inclusion trails. (C) BSE image of staurolite-grade schist. (D) BSE image of staurolite-grade schist. Note ilmentite concentrated at chlorite-biotite boundaries and chlorite overgrowing biotite parallel to a chevron fold axis. (E) Plane polarized light photomicrograph of garnet/biotite-grade schist. (F) BSE image of garnet/biotite-grade schist. (G, H) BSE images of biotite-grade schists. (I) Plane polarized light photomicrograph of chlorite-grade phyllite. (J, K) BSE images of chlorite-grade phyllite. (L) BSE image of chlorite-grade phyllite. Abbreviations: biotite (bt), carbon (crb), chlorite (chl), garnet (grt), ilmenite (ilm), muscovite (ms), staurolite (str), quartz (qtz).

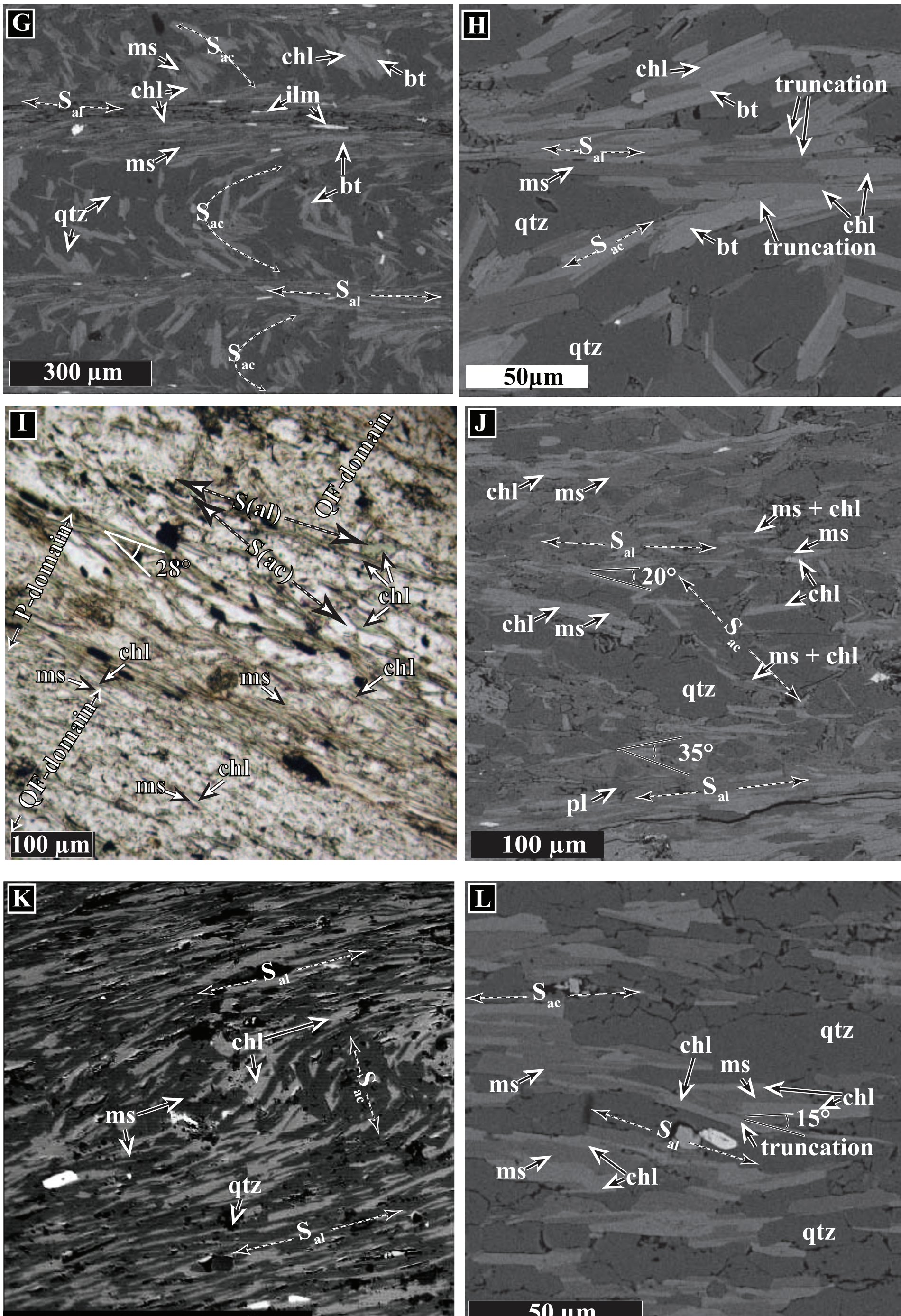

Fig. 3 (continued).

high-grade metamorphism and are thus designated S(ac) (for example, fig. 3A). The dominant, penetrative Acadian fabric is given the symbol S(ac). Other older or younger Acadian fabrics are denoted S(ac+1), S(ac-1), *et cetera,* where the designation S(ac-1) indicates that the fabric predates S(ac) by one generation and the designation S(ac+1) indicates that the fabric postdates S(ac) by one generation but is not Alleghanian in age. No attempt has been made here to correlate individual schistosities with those mapped in the field, as our field observations suggest that most schistosities are transposed into a single composite foliation.

Microstructures.—The Wepawaug Schist is characterized by multiple matrix fabrics that developed in three stages: prograde, high-grade, and retrograde. Earlier schistosities defined by prograde mineral assemblages preserved within porphyroblasts but not within the matrix (for example, figs. 3A and 3B) are not discussed here (but see Bell and Newman, 2006). High-grade rocks contain cleavages defined by biotite-muscovite intergrowths (for example, figs. 3A and 3B, figs. 3G and 3H) that may wrap around garnet and staurolite porphyroblasts where present (for example, curved, dashed arrows, figs. 3A and 3B). Late, retrograde, crosscutting chlorite-muscovite fabrics are pervasive, and locally penetrative, throughout the OMB. These texturally late cleavages cross cut older cleavages defined by muscovite + biotite, muscovite + biotite + chlorite, and/or muscovite + chlorite ("truncation," fig. 3). This late fabric is the dominant schistosity in some rocks [for example, S(al) fig. 3E], whereas in others it is only weakly present [for example, S(al) figs. 3A and 3B]. It is, however, ubiquitous, being at least weakly developed in over 100 samples studied and is therefore regionally pervasive.

Matrix fabrics in staurolite/kyanite-grade phyllites.—Fine-grained gray-green muscovite schists with abundant biotite and 3 to 10 mm garnet and staurolite porphyroblasts typify the high-grade Wepawaug Schist. Kyanite laths up to 2 cm long can be found where the bulk composition is appropriate. Garnet and staurolite porphyroblasts are pseudomorphically replaced by muscovite + chlorite intergrowths. For instance, sample JAW35A is a gray phyllite with sub mm-scale inclusion-rich garnet and staurolite porphyroblasts (figs. 3A and 3B). Intergrown muscovite and biotite define a dominant matrix schistosity, S(ac), that wraps around the porphyroblasts (fig. 3B). Quartz and carbon inclusion trails in garnet and staurolite are oriented at a high angle to and are truncated by S(ac) (figs. 3A and 3B). Biotite grains are at least twice as large as muscovite grains in this schistosity but muscovite is about three times more abundant than biotite (figs. 3A-3C). The S(ac) fabric truncates an older biotite-rich fabric [S(ac-1), "truncations," figs. 3A and 3C] in which individual biotite grains are up to $\sim$1000 μm long and $\sim$50 μm wide. These biotite grains define sharp chevron folds, the axes of which are the approximate locus for growth of new phyllosilicates ("chevron folded bt," fig. 3D). The younger fabric, S(al) is defined by intergrowths of chlorite and muscovite locally associated with ilmenite [for example, S(al), figs. 3C and 3D]. It is difficult to identify S(al) as a distinct fabric optically even though large chlorite grains are visible ("chl," fig. 3A), but backscattered-electron (BSE) imaging clearly shows S(al) truncating micas that define older fabrics (figs. 3C-3D). The occurrence of ilmenite with the late chlorite + muscovite fabrics (fig. 3D) is consistent with the higher solubility of Ti in biotite than in the replacing muscovite + chlorite (for example, table 1). Thus ilmenite is a reaction bi-product of the of the retrograde replacement of biotite by S(al)-defining muscovite and chlorite.

Matrix fabrics in biotite-grade phyllites.—Fine-grained gray-green muscovite schists with common porphyroblasts of biotite and 1 to 7 mm garnet that may be partially replaced by chlorite characterize the biotite-garnet-grade rocks of the Wepawaug Schist. Sample CT0701 (figs. 3E-3F) is typical of these rocks. It is a gray phyllite from the upper garnet zone (fig. 1B) in which all garnets were pseudomorphically replaced

Table 1

Representative electron microprobe analyses of muscovite, biotite, and chlorite for selected samples from the Orange-Milford Complex

	Muscovite								Chlorite										Biotite					
Sample no.		CT0713		CT0701		JAW49A		JAW35A		CT0713		CT0723		CT0701		JAW49A		JAW35A		CT0701		JAW49A		JAW35A
SiO_2		47.42		47.55		46.66		46.72		25.43		25.45		25.87		25.35		25.76		36.01		36.30		37.30
Al_2O_3		34.82		37.50		35.37		38.03		23.67		22.08		23.02		22.65		23.24		18.59		18.53		19.99
TiO_2		0.41		0.38		0.39		0.48		0.07		0.06		0.07		0.10		0.09		1.76		1.70		1.43
FeO		1.95		1.48		1.95		0.98		25.49		30.12		25.79		26.34		23.41		20.84		20.80		15.98
MnO		0.06		0.01		0.00		0.01		0.27		0.32		0.17		0.34		0.02		0.11		0.14		0.03
MgO		1.64		0.92		1.18		0.74		15.69		12.79		15.85		15.68		17.20		10.66		10.72		12.66
CaO		0.02		0.01		0.05		0.01		0.00		0.02		0.01		0.02		0.02		0.07		0.01		0.01
Na_2O		0.52		0.35		0.55		1.44		0.02		0.00		0.00		0.00		0.00		0.05		0.04		0.24
K_2O		9.62		8.57		9.85		8.13		0.13		0.04		0.01		0.10		0.07		8.22		9.21		8.54
Total		96.45		96.78		96.00		96.53		90.78		90.88		90.79		90.58		89.81		96.31		97.44		96.18
Si	8.00	6.22	8.00	6.14	8.00	6.16	8.00	6.05	4.00	2.58	4.00	2.65	4.00	2.63	4.00	2.60	4.00	2.61	8.00	5.42	8.00	5.42	8.00	5.47
Al		1.78		1.86		1.84		1.95		1.42		1.35		1.37		1.40		1.39		2.59		2.58		2.53
Al		3.60		3.85		3.66		3.85		1.42		1.35		1.38		1.33		1.39		0.71		0.68		0.92
Ti		0.04		0.04		0.04		0.05		0.01		0.00		0.01		0.01		0.01		0.20		0.19		0.16
Fe	4.18	0.21	4.22	0.16	4.15	0.22	4.15	0.11	5.98	2.16	5.99	2.62	5.99	2.19	6.02	2.26	5.99	1.99	5.93	2.62	5.87	2.60	5.81	1.96
Mn		0.01		0.00		0.00		0.00		0.02		0.03		0.01		0.03		0.00		0.01		0.02		0.00
Mg		0.32		0.18		0.23		0.14		2.37		1.98		2.40		2.39		2.60		2.39		2.39		2.77
Ca		0.00		0.00		0.01		0.00		0.00		0.00		0.00		0.00		0.00		0.01		0.00		0.00
Na	1.75	0.13	1.5	0.09	1.81	0.14	1.71	0.36	0.02	0.00	0.01	0.00	0.00	0.00	0.01	0	0.01	0.00	1.61	0.02	1.87	0.012	1.67	0.07
K		1.61		1.41		1.66		1.34		0.02		0.01		0.00		0.01		0.01		1.58		1.75		1.60
Total		13.92		13.72		13.95		13.86		10.01		10.00		9.99		10.03		10.00		15.54		15.64		15.48
Fe/(Fe+Mg)		0.40		0.47		0.48		0.43		0.48		0.57		0.48		0.49		0.43		0.52		0.52		0.41

Cations calculated on the basis of 24-muscovite, 18-chlorite and 24-biotite oxygen atoms.

by fine-grained, randomly oriented muscovite and chlorite. Muscovite and chlorite also form a dominant late crenulation fabric in this sample (S(al), figs. 3E-3F) that crosscuts all other fabrics. This fabric forms at a low angle to elongated biotite porphyroblasts up to 500 μm long and 100 μm wide that weakly define the oldest fabric [S(ac), fig. 3E]. These biotite grains occur as large laths containing quartz inclusions (fig. 3F). The biotite laths that define S(ac-1) can be truncated at a high angle by muscovite grains ~150 μm × 30 μm that are aligned parallel to additional biotite flakes measuring ~200 μm × 40 μm ("truncation" lower left, fig. 3E). These grains define a zonal muscovite + biotite fabric (S(ac), fig. 3E) that meets and is truncated by the late muscovite + chlorite S(al) fabric at ~15–45° (figs. 3E-3F). This late fabric also cross-cuts the older inclusion-rich biotite laths ("truncation," fig. 3F) where ilmenite may ornament the grain boundary. The ilmenite is likely a product of the retrograde formation of the crosscutting muscovite + chlorite fabric.

A typical sample collected at the biotite isograd (JAW49A, fig. 1B) is a gray phyllite characterized by a strong, discrete crenulation cleavage in which muscovite and biotite grains in the microlithons define a folded fabric [S(ac), fig. 3G]. Although this fabric is folded, individual muscovite and biotite grains, typically ~120 μm long and 18 to 50 μm wide, are straight rather than bent [S(ac), fig. 3G] suggesting that folding was syn-metamorphic. Biotite in other microlithons is intimately intergrown with chlorite (figs. 3G-3H). A younger fabric of aligned and intergrown ilmenite laths with muscovite and chlorite flakes, up to 200 μm long and about 30 to 50 μm thick, truncates the earlier cleavage [S(al), fig. 3H]. Ilmenite, again apparently a product of a retrograde reaction, is oriented parallel to the long dimension of the phyllosilicate flakes (fig. 3G).

Fabrics in chlorite-grade phyllites.—Fine-grained gray-green muscovite-chlorite phyllites characterize the lowest-grade Wepawaug Schist. For example, samples CT0713 and CT0723 (fig. 1B) are gray-green phyllites with alternating quartz- and albite-rich QF-domains and phyllosilicate-rich P-domains (fig. 3I). In thin section, zonal crenulation cleavages defined by fine-grained, ~100 μm long, aligned chlorite and muscovite grains are conspicuous (fig. 3I). Phyllosilicate-rich P-domains, typically approximately 200 to 500 μm across and composed of >90 percent phyllosilicates and <10 percent quartz and albite, contain two fabric orientations at ~15 to 45° to each other (figs. 3I-3K). The most well-developed and continuous fabric in these domains is composed of muscovite and chlorite flakes with aspect ratios greater than 10:1 [S(al), figs. 3I-3K]. An older S(ac) fabric grades into and is truncated against this continuous S(al) fabric and contains muscovite and chlorite flakes with aspect ratios typically about 5:1 (note "35°" angle, fig. 3J). Both of these fabrics are also preserved in the >300 μm wide quartz- and albite-rich QF-domains that contain ~80 percent quartz and albite and 20 percent phyllosilicates; however, here the truncated S(ac) fabric is better developed than the truncating S(al) fabric (fig. 3L).

Mineral Chemistry

Representative electron microprobe analyses for muscovite, chlorite, and biotite are presented in table 1, and all analyses are summarized in figure 4. Compositions of muscovite, chlorite, and biotite in these samples fall within the range of typically accepted values for these minerals (table 1) and figure 4 shows minimal to moderate solid solution for each mineral.

Muscovite compositions.—Muscovite chemical analyses from six samples reveal compositional variations in which octahedral Al varies inversely with other octahedral cations (Fe, Mg, Mn, and Ti) (fig. 4A). Though analyses from individual samples define more restricted compositional variations, all 132 analyses form a trend with a slope of ~ -1 (fig. 4A) as expected from Tschermakitic substitution of Al into the octahedral site given by $^{VI}X^{2+} + {}^{IV}Si^{4+} = {}^{VI}Al^{3+} + {}^{IV}Al^{3+}$ (Dymek, 1983). The smaller

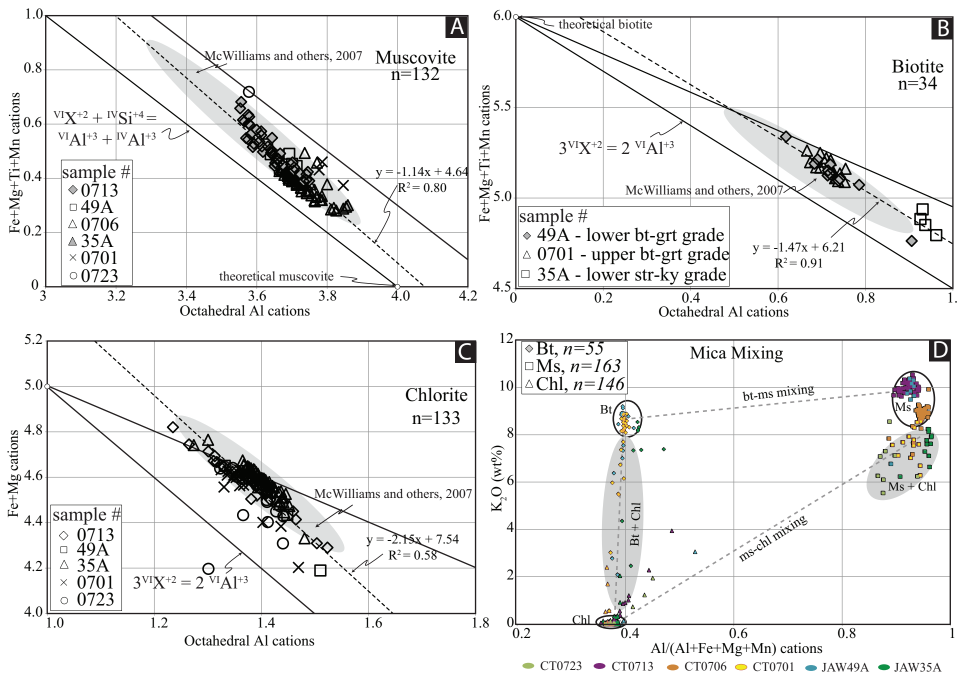

Fig. 4. Compositions of muscovite, chlorite and biotite from representative samples showing ranges of solid solution. Solid lines represent ideal substitutions whereas dashed lines are best-fit lines. Equations of each best-fit line are given. (A) Electron microprobe analyses of muscovite from six samples form a linear solid-solution trend with slope of ~ -1. (B) Electron microprobe analyses of biotite from three samples form a linear solid-solution trend with a slope of ~ -1.5. (C) Electron microprobe analyses of chlorite from five samples form a poor linear trend with a slope of ~ -2. (D) Electron microprobe analyses of biotite, chlorite, and muscovite. Mixing lines between end-member phases (white circles) are indicated by dashed gray lines. Biotite-chlorite solid solution is nearly continuous (large gray oval), while mixed muscovite-chlorite compositions are more restricted.

compositional variation of individual samples likely reflects local, relatively restricted bulk composition differences among the samples.

Biotite compositions.—Biotite analyses commonly have low weight percent K_2O (<8%) due to the presence of very finely intergrown chlorite (for example, figs. 3G-3H, and 4D). Those analyses with acceptable K_2O content (>8%) show similar trends to those identified in the muscovite data in that the octahedral Al varies inversely with the other octahedral cations (Fe, Mg, Mn and Ti) (fig. 4B). Unlike the muscovite, however, the biotite analyses define a trend with a slope of ~ -1.5 (fig. 4B) consistent with a di/trioctahedral substitution where $2\ {}^{VI}Al^{3+} = 3\ {}^{VI}X^{2+}$ (Dymek, 1983). It is interesting to note that an increase in octahedral Al content relative to the other octahedral cations appears to correlate with the transition from garnet-biotite to staurolite grade (fig. 4B) but the data are too limited to draw conclusions from this apparent trend.

Chlorite compositions.—Solid-solution trends in chlorite analyses are similar to those identified in both biotite and muscovite in that concentrations of octahedral Al vary inversely with Fe + Mg (fig. 4C). The overall trend in the data defines a slope of ~ -2. As with biotite, this suggests that the di/trioctahedral substitution of Dymek (1983) dominates over the Tschermakitic substitution. Muscovite, chlorite, and biotite analyses plotted together reveal evident mixing between pure mica compositions (fig. 4D).

Chlorite-biotite mixing follows a nearly continuous linear mixing line of decreasing K_2O content from biotite (>8 wt% K_2O) to chlorite (0 wt% K_2O) (fig. 4D). This mixing is probably due to partial chloritization of biotite. The analytical data provide little evidence for fine-scale intergrowths of biotite with muscovite. Muscovite and chlorite compositions follow a linear mixing line of increasing K_2O content with Al/(Al+Fe+Mn+Mg) (fig. 4D). These analyses provide evidence of fine muscovite-chlorite and biotite-chlorite intergrowths that occur at a scale finer than the 3-μm electron beam used for chemical analysis. The apparent mixing of the phyllosilicate chemistries (fig. 4D) shows that the electron beam overlapped intergrowths of two micas that were too small to be resolved on the thin-section scale yet were observed with the SEM (for example, fig. 3H).

Compositional zoning.—Analyses of single phyllosilicate grains from all samples show that grains in each sample are chemically zoned. Zoning trends define climbing, bell- or U-shaped arcuate, or oscillatory patterns. Muscovite typically displays bell-shaped patterns of higher phengite content in the core decreasing to lower phengite content near the rim (figs. 5A and 5B). This pattern is observed in both S(al) and S(ac) fabric-forming muscovites (for example, I-III; figs. 5A and 5B) and is more commonly observed than other patterns (8 of 13 grains). Muscovite grains can also display oscillatory patterns (1 of 13 grains, for example, IV; figs. 5A and 5B), climbing patterns (3 of 13 grains), and U-shaped patterns (2 of 13 grains). Climbing and oscillatory patterns are much more common among biotite grains (4 each out of 11 grains, for example, fig. 5C) and oscillatory patterns dominated chlorite grains (8 of 9 grains, for example, fig. 5D). Muscovite and chlorite grains were typically not wide enough to allow more than one traverse per grain to identify two-dimensional zoning patterns. A biotite grain from sample CT0701 was large enough for three traverses (fig. 5E). Chemical analyses of this grain reveal a band of high octahedral Al cation content cutting obliquely across the grain. This pattern is mirrored with a complementary decrease in $^{VI}X^{2+}$ cations (fig. 5F) as expected of the di/trioctahedral substitution (Dymek, 1983) in these biotite (see fig. 4).

Compositional zoning in phyllosilicates.—Compositional zoning was identified in all three fabric-forming phyllosilicates—muscovite, biotite, and chlorite—and the range of compositions found here is comparable with those reported by McWilliams and others (2007) (see figs. 4A-4C). Compositional variations are commonly homogenized by accelerated intra-crystalline diffusion during metamorphism so the zoning found in these grains must represent a minimum amount of zoning present during growth of the phyllosilicates. The range of muscovite compositions in both S(al) and S(ac) fabrics completely overlaps in five of the six samples studied (for example, fig. 6A). Such phyllosilicate zoning patterns cannot be produced by stepped growth at distinct PT conditions, but must be produced by continuous, progressive growth from a fluid reservoir during metamorphism. Furthermore, zoning in muscovites preserves a decrease in phengite content from core to rim, implying that muscovites grew during retrograding conditions (for example, Currie and others, 2003).

It is likely that the Wepawaug Schist experienced high volumes of fluid flux at some stage during prograde metamorphism (Ague, 2000, 2003) and fluid flow must take place through rocks during diagenesis and early metamorphism (for example, Oliver, 1996) due to compaction of fluid-filled pores and dehydration reactions. The presence of prograde- and high-grade mineral assemblages identified in the field and interpreted to have formed due to fluid flow (Ague, 2003) suggests that, in this case, the fluids were present during higher-grade conditions. These fluids are proposed to have escaped the rocks along veins, with a component of along-fabric flow (Ague, 1994b).

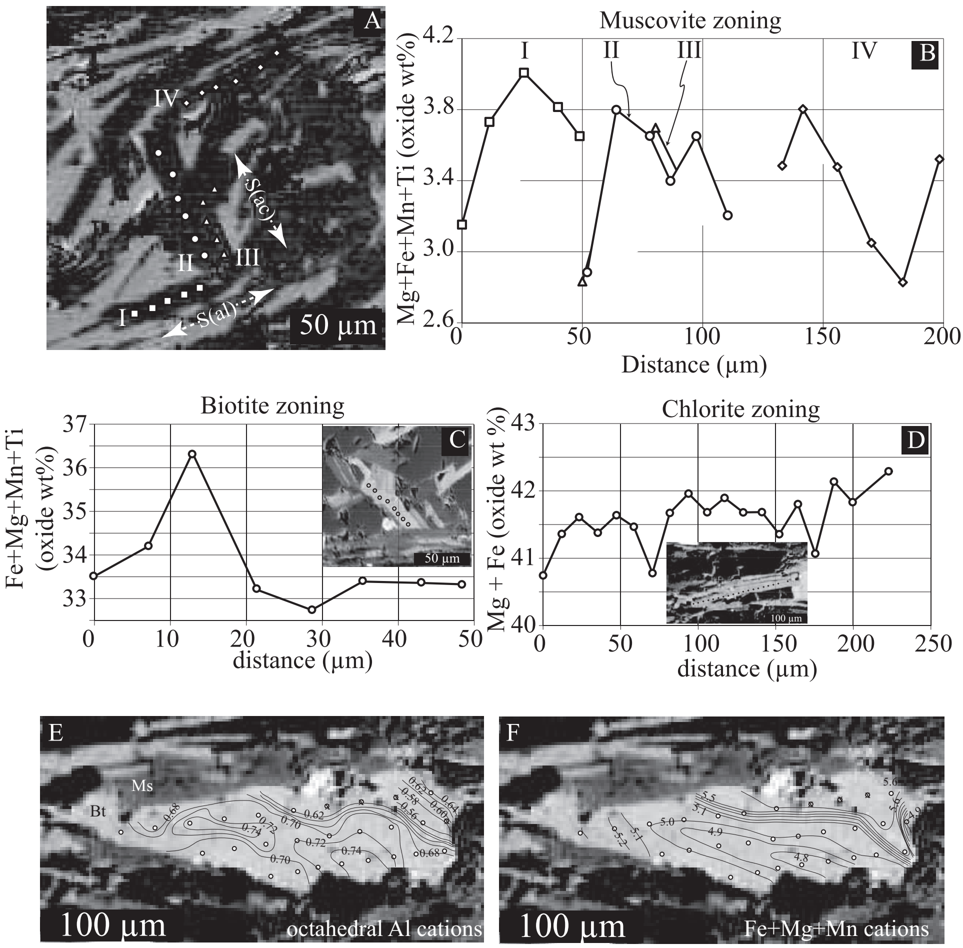

Fig. 5. Backscattered electron images and diagrams showing typical zoning patterns of phyllosilicates from schists in the OMB. (A) BSE image of chlorite-grade phyllite showing locations of electron microprobe analyses (white diamonds, squares, triangles and circles drawn to scale of 3 µm electron microprobe analysis spot) along four (I-IV) muscovite grains (dark gray). (B) Zoning patterns from single muscovite grains shown in (A). (C) Oscillatory zoning patterns are common in biotite grains, and climbing-oscilating patterns are common in chlorite grains (D). (E, F) Cation zoning evident in electron microprobe analytical traverses across a biotite grain.

Generally, minerals that crystallize from large fluid reservoirs, or from reservoirs that are continually refreshed, develop little zoning, whereas minerals that crystallize from smaller, more restricted fluid reservoirs will develop more pronounced zoning (McWilliams and others, 2007). If cleavage-defining phyllosilicates crystallized from a large fluid reservoir their zoning would be muted; however, the presence of ubiquitous zoning in the phyllosilicates analyzed here suggests crystallization from small and fractionating fluid reservoirs (McWilliams and others, 2007) and supports the existence of several, chemically distinct, cleavage-forming phyllosilicate populations in these rocks. Furthermore, muscovite in muscovite-chlorite cleavages that developed during lower-greenschist-facies temperatures should preserve $^{40}Ar/^{39}Ar$ crystallization ages.

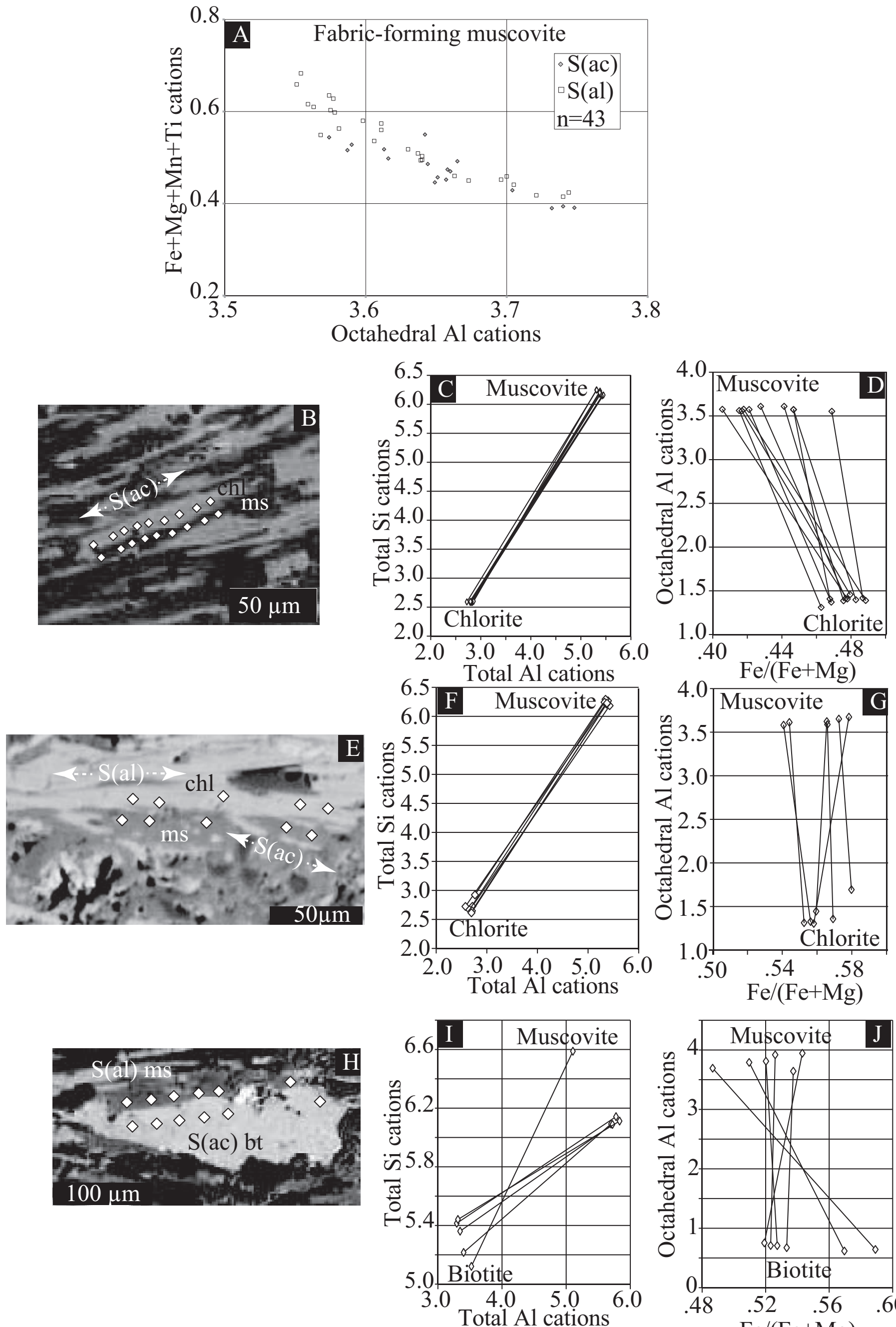

Fig. 6. Compositional variations within phyllosilicates. Locations of analysis traverses are shown in SEM images with white diamonds. (A) Electron microprobe analyses of muscovite grains from sample CT0713 showing overlapping compositions of S(ac) (gray diamonds) and S(al) (white squares). (B) BSE image of S(ac)-defining muscovite (ms, dark gray) and chlorite (chl, light gray) from sample CT0713. Parallel (C) and smoothly fanning (D) tie lines join pairs of muscovite and chlorite analyses from (B). (E) BSE image of S(al)-defining chlorite grain (chl, light gray) truncating S(ac) muscovite grain (ms, dark gray) from sample CT0723. Parallel (F) and crossing (G) tie lines joining pairs of muscovite and chlorite analyses from (E). (H) BSE image of S(al)-defining muscovite grain (ms, dark gray) truncating S(ac) biotite grain (bt, light gray) from sample CT0701B. Crossing (I, J) tie lines joining pairs of muscovite and biotite analyses from (H).

The extent to which co-crystallizing cleavage-forming phyllosilicates in these rocks were in equilibrium with each other and the fluid reservoir is evaluated in figure 6. The Si and Al contents of adjacent muscovite and chlorite grains in sample CT0713 (fig. 6B) vary sympathetically. In all cases lines connecting mineral pairs have parallel and positive slopes consistent with equilibrium crystallization from a common grain boundary fluid (fig. 6C). Similarly tie-lines comparing octahedral Al content with Fe/(Fe+Mg) (fig. 6D) form a smooth fanning pattern showing that the range of Fe/(Fe + Mg) in chlorite is much narrower than in muscovite, consistent with equilibrium crystallization during cleavage development.

In contrast, cleavage-forming grains that truncate earlier grains and fabrics are interpreted based on textures to have crystallized at different times; these grain pairs do not display this same equilibrium partitioning (for example, figs. 6E-6J). Indeed, the crossing tie lines indicate disequilibrium between minerals along a common grain boundary and further support the presence of multiple cleavage generations in these rocks. Disequilibrium between crosscutting minerals defining different cleavages suggests that the minerals crystallized from fluid reservoirs with distinct chemistries. These minerals most likely crystallized from different fluid reservoirs that were present at different *times.* Therefore minerals oriented parallel to one another and which share grain boundaries crystallized together during a common event, whereas minerals oriented at angles to, and crosscutting each other, crystallized during chemically and temporally distinct cleavage-forming events. Cleavage-defining phyllosilicates should, therefore, preserve the times of their crystallization if they have not been thermally reset. The newly recrystallized cross cutting muscovite + chlorite cleavages within these rocks are expected to preserve post-Acadian crystallization ages.

^{40}Ar/^{39}Ar Results

Muscovite and amphibole from the field area were dated using the ^{40}Ar/^{39}Ar step-heating method to provide a chronological context for cooling from regional metamorphism. To this end, five amphibole and 14 muscovite separates were analyzed. Analytical data are given in table 2, a summary of the interpreted ages is given in table 3, and age spectra and inverse isochron diagrams are presented in figures 7 and 8.

Amphibole.—All amphibole samples were collected from amphibolites or, west of the EDSZ, amphibole-bearing orthogneisses that experienced at least staurolite-grade metamorphic conditions (see fig. 1B). These rocks contain >40 percent medium- to coarse-grained amphibole coexisting with, and typically including, plagioclase, epidote, magnetite, biotite, garnet, titanite, and calcite. The amphiboles in all samples define at least weak foliations evident at the outcrop and thin-section scales. All amphibole separates were prepared at grain sizes small enough to avoid inclusions visible with a binocular microscope. The purity of the sample separates is confirmed by the nearly constant K/Ca ratios shown with the age spectra (figs. 7A-7E). However, ages of the lowest-temperatures steps for which the K/Ca ratios were typically disturbed were discounted due to the likely presence of very small inclusions in the samples.

The age spectra produced by several amphiboles are disturbed by excess argon or other contamination (for example, figs. 7A-7C) and in one sample the results are uninterpretable (fig. 7A). In some of these samples the inverse isochron diagrams suggest the presence of excess ^{40}Ar and the cooling age is interpreted to be either the minimum age step or the inverse isochron age. In several cases the minimum age step and the inverse isochron age agree within error. In two cases the amphibole spectra give plateau ages that agree within error with the inverse isochron ages (figs. 7D-7E).

The time of cooling through ~500 °C (Mcdougall and Harrison, 1999) is estimated by plateau or inverse isochron ages from three samples (table 3, figs. 7C-7E) to

Table 2

Summary of Ar data produced from samples studied

Step	T°C	K/Ca	K/Cl	$^{40}Ar^*/^{39}Ar$	^{39}Ar (% total)	$\%^{40}Ar^*$	Age (Ma)	± Age
Sample JAW35A muscovite, staurolite zone (J=0.009167±0.000023)								
A	600	4.77	24	35	0.48	16.8	175.58	3.28
B	700	14.48	204	36.471	2.38	86.8	228.37	0.67
C	800	29.23	488	16.984	5.8	98.0	310.98	0.56
D	850	34.08	1496	16.107	6.1	98.9	320.13	0.72
E	900	47.09	2678	11.567	8.6	98.9	331.44	0.61
F	950	103.06	10115	5.259	18.9	99.4	343.55	0.61
G	1000	78.36	13147	6.147	16.2	99.4	343.05	0.50
H	1050	31.32	3735	11.074	8.9	99.0	343.33	0.61
I	1100	22.46	2398	12.222	8.1	99.0	341.92	0.77
J	1150	18.02	1938	8.701	11.3	98.5	349.50	0.59
K	1200	18.22	185	8.557	11.6	99.0	355.14	0.62
L	1250	2.44	95	65.473	1.48	96.9	357.38	1.51
M	1350	0.26	36	417.368	0.19	79.3	335.29	6.33
Sample CT0703A muscovite, staurolite zone (J=0.009208±0.000023)								
A	600	6.39	11	83.333	0.1	10.0	250.26	5.52
B	700	11.23	101	192.105	0.4	73.0	302.03	1.23
C	800	43.54	264	78.167	1.2	93.8	341.86	1.03
D	850	157.64	738	54.237	1.8	96.0	345.38	0.49
E	900	262.90	1259	32.033	3.0	96.1	345.16	0.45
F	950	555.87	1208	14.438	6.5	93.7	350.21	0.52
G	1000	9299.45	1853	3.957	24.1	95.2	349.84	0.19
H	1050	687.78	6254	7.139	13.8	98.3	343.27	0.50
I	1100	276.17	2395	16.090	6.0	96.7	342.77	0.47
J	1150	242.96	1654	18.500	5.2	96.2	344.05	0.48
K	1200	475.92	819	9.514	10.1	96.0	346.03	0.38
L	1250	906.76	801	5.185	19.0	98.3	348.59	0.29
M	1350	235.52	1280	15.280	6.4	98.4	342.43	0.63
N	1450	76.74	643	45.115	2.2	97.9	341.53	0.43
O	1650	16.30	103	269.714	0.4	94.4	342.18	1.80
Sample CT0715 muscovite, staurolite zone (J=0.009190±0.000023)								
A	600	5.71	11	49.474	0.2	9.4	177.79	8.06
B	700	11.84	96	126.032	0.6	79.4	259.95	1.30
C	800	54.12	391	46.845	2.1	96.5	310.33	0.61
D	850	133.04	1224	34.804	2.8	97.8	315.34	0.55
E	900	279.79	2738	15.584	6.3	97.4	325.41	0.56
F	950	1058.50	35888	3.375	29.4	99.2	336.84	0.17
G	1000	325.38	40159	6.613	15.0	99.2	326.05	0.43
H	1050	136.68	5314	15.391	6.4	98.5	319.34	0.48
I	1100	93.52	2718	18.705	5.3	98.2	323.53	0.45
J	1150	64.57	2873	13.401	7.4	98.5	329.31	0.50
K	1200	262.42	596	5.565	17.8	99.0	334.30	0.39
L	1250	108.66	1150	16.947	5.8	98.8	339.61	0.65
M	1350	27.58	133	92.347	1.0	90.5	339.11	1.24
N	1450	3.50	37	1211.429	0.1	84.8	353.66	11.62
Sample CT0701B muscovite, biotite zone (J=0.009231±0.000023)								
A	600	5.31	17	27.907	0.43	12	148.72	6.08
B	700	9.25	125	38.945	1.99	77.5	196.57	1.46
C	800	16.54	310	21.518	4.5	96.4	292.23	0.65
D	850	23.86	989	16.775	5.9	98.3	310.89	0.75
E	900	25.25	2340	10.614	9.3	98.6	316.52	0.40
F	950	35.11	7817	7.025	14.1	99.2	325.00	0.56
G	1000	69.93	25656	4.790	20.8	99.4	332.04	0.46
H	1050	38.85	5467	7.188	13.8	99.2	331.75	0.50
I	1100	20.65	2189	10.259	9.6	98.9	332.80	0.54
J	1150	15.35	1714	8.077	12.2	98.7	340.16	0.52
K	1200	9.80	90	14.211	6.8	97.2	346.77	0.52
L	1250	0.59	21	177.333	0.45	79.8	321.93	4.62
M	1350	0.22	9	383.571	0.14	53.7	380.36	12.78

Table 2

(continued)

Step	T°C	K/Ca	K/Cl	$^{40}Ar^{*}/^{39}Ar$	^{39}Ar (% total)	$\%^{40}Ar^{*}$	Age (Ma)	± Age
Sample JAW35A muscovite, staurolite zone (J=0.009167±0.000023)								
A	600	5.77	39	34.800	0.5	17.4	87.13	4.05
B	700	12.14	196	49.766	1.7	85.1	193.79	0.91
C	800	19.47	408	20.332	4.8	98.0	280.57	0.72
D	850	19.19	1375	18.731	5.3	98.9	311.58	0.64
E	900	17.70	2777	13.284	7.5	99.1	317.86	0.57
F	950	23.00	9212	8.134	12.2	99.4	327.33	0.62
G	1000	44.37	30927	5.118	19.4	99.5	333.42	0.56
H	1050	49.39	13051	6.642	15.0	99.5	334.45	0.34
I	1100	36.44	4807	9.103	10.9	99.4	336.44	0.61
J	1150	28.51	5265	6.286	15.8	99.5	342.80	0.58
K	1200	9.09	123	15.333	6.5	98.9	350.60	0.64
L	1250	0.68	85	248.158	0.4	94.3	365.81	3.40
Sample CT0708 muscovite, biotite zone (J=0.009214±0.000023)								
A	600	15.00	61	28.158	1.1	32.1	106.91	1.25
B	700	23.24	272	27.699	3.4	93.9	242.22	0.51
C	800	57.19	775	12.844	7.7	98.9	312.28	0.53
D	850	72.58	2337	13.315	7.5	99.2	315.38	0.54
E	900	85.38	6715	10.621	9.3	99.2	317.83	0.43
F	950	123.51	31092	7.525	13.2	99.4	326.03	0.42
G	1000	167.84	**	5.676	17.5	99.5	330.95	0.25
H	1050	128.13	25285	6.667	14.9	99.4	334.90	0.65
I	1100	60.42	4662	9.020	11.0	99.4	340.22	0.49
J	1150	55.62	2599	9.355	10.5	98.6	344.28	0.57
K	1200	28.04	79	28.517	3.4	98.1	349.75	0.73
L	1250	2.83	25	306.071	0.3	85.7	366.11	4.32
M	1350	1.10	9	868.333	0.1	52.1	446.91	16.06
Sample CT0714 amphibole, staurolite zone (J=0.009225±0.000023)								
A	700	0.11	7	268.065	0.3	83.1	2669.84	4.69
B	800	0.30	45	100.787	0.9	89.7	709.50	1.51
C	900	0.23	91	72.804	1.1	77.9	444.03	1.14
D	1000	0.06	155	23.721	3.4	81.6	376.03	0.71
E	1050	0.03	175	26.958	3.3	89.5	445.67	0.94
F	1075	0.06	242	14.389	6.4	91.8	434.22	0.68
G	1100	0.06	349	5.606	17.3	97.1	432.98	0.17
H	1125	0.07	462	7.583	12.9	97.9	394.73	0.36
I	1150	0.06	80	28.024	3.3	92.2	392.66	1.06
J	1175	0.07	205	8.933	10.6	94.6	404.99	0.57
K	1200	0.07	320	6.119	15.7	96.0	414.92	0.55
L	1225	0.07	393	5.174	18.9	98.0	418.48	0.69
M	1250	0.06	398	18.953	5.2	97.8	399.34	0.60
N	1450	0.04	164	130.00	0.7	89.7	404.17	1.07
Sample CT0726 amphibole, staurolite zone (J=0.00924±0.000023)								
A	700	0.13	5	222.800	0.3	55.7	1463.36	4.96
B	800	0.22	32	77.789	1.0	73.9	385.50	2.32
C	900	0.14	50	63.789	1.0	60.6	351.23	1.42
D	1000	0.04	77	24.335	3.2	76.9	371.60	1.32
E	1050	0.04	92	18.578	4.5	83.6	377.08	0.68
F	1075	0.04	116	4.415	20.5	90.6	376.44	0.63
G	1100	0.04	136	3.766	25.3	95.4	377.53	0.36
H	1125	0.05	132	11.244	8.5	95.8	374.09	0.51
I	1150	0.04	22	51.313	1.6	82.1	367.77	0.98
J	1175	0.04	61	21.634	4.1	88.7	381.90	0.77
K	1200	0.04	116	10.618	8.7	92.8	388.41	0.71
L	1225	0.04	117	9.465	10.1	95.5	402.91	0.49
M	1250	0.04	126	10.104	9.6	96.9	396.95	0.62
N	1450	0.04	109	54.529	1.7	92.7	391.69	1.44
50.35 % gas released in plateau steps					Plateau age		377.23	0.863

Table 2

(continued)

Step	T°C	K/Ca	K/Cl	$^{40}Ar^{*}/^{39}Ar$	^{39}Ar (% total)	$\%^{40}Ar^{*}$	Age (Ma)	± Age
Sample CT0712 amphibole, staurolite zone (J=0.009225±0.000023)								
A	700	0.09	5	201.000	0.1	20.1	611.61	8.02
B	800	0.24	27	278.095	0.2	58.4	331.74	3.15
C	900	0.15	45	101.429	0.5	49.7	327.52	1.73
D	1000	0.07	100	19.091	4.1	77.7	369.52	0.63
E	1050	0.06	126	16.762	5.2	87.5	373.91	0.62
F	1075	0.08	151	4.679	20.1	94.1	374.09	0.40
G	1100	0.08	165	3.063	31.7	97.2	374.26	0.33
H	1125	0.09	163	8.352	11.6	96.8	375.64	0.42
I	1150	0.08	102	34.610	2.7	93.1	376.67	0.86
K	1200	0.08	125	13.305	7.1	94.2	376.36	0.59
L	1225	0.09	147	20.083	4.8	96.4	377.00	0.73
M	1250	0.09	164	21.419	4.6	98.1	377.91	0.72
N	1450	0.09	157	24.822	3.9	97.8	377.94	0.59
O	1650	0.09	110	274.194	0.3	85.0	373.89	3.27
68.65 % gas released in plateau steps					Plateau age		374.51	0.852
Sample CT0714B muscovite, staurolite zone (J=0.009186±0.000023)								
A	600	3.57	25	129.231	0.1	16.8	148.95	3.13
B	700	6.49	83	244.848	0.3	80.8	271.16	1.59
C	800	29.44	232	82.845	1.2	96.1	316.49	0.90
D	850	60.68	877	56.959	1.7	97.4	318.22	0.81
E	900	123.10	1946	31.934	3.1	97.4	320.12	0.76
F	950	630.48	12059	6.626	14.9	98.6	329.98	0.31
G	1000	568.02	**	3.857	25.8	99.4	327.33	0.36
H	1050	195.37	7080	12.265	8.1	99.1	323.89	0.86
I	1100	150.03	5044	16.203	6.1	99.0	326.09	0.66
J	1150	160.83	5358	14.265	6.9	99.0	328.40	0.53
K	1200	346.63	363	8.363	11.9	99.1	329.45	0.55
L	1250	290.16	1942	8.454	11.8	99.5	329.00	0.57
M	1350	166.01	4961	17.378	5.7	99.4	333.48	0.55
N	1450	104.81	2096	39.562	2.5	99.3	335.22	0.44
Sample CT0706 muscovite, staurolite zone (J=0.009173±0.000023)								
A	600	4.94	24	91.500	0.2	18.3	172.23	5.73
B	700	10.84	143	121.014	0.7	83.5	249.22	1.40
C	800	35.31	380	44.259	2.2	95.6	296.18	0.93
D	850	49.13	1211	32.584	3.0	97.1	301.31	0.69
E	900	55.12	1948	17.227	5.6	96.3	307.46	0.51
F	950	174.45	13960	3.720	26.5	98.7	319.02	0.32
G	1000	97.57	23981	5.391	18.4	99.2	310.38	0.41
H	1050	63.41	5849	11.673	8.4	98.4	302.22	0.37
I	1100	71.08	2607	17.865	5.5	97.9	306.01	0.60
J	1150	69.67	2333	13.890	7.1	98.2	310.87	0.40
K	1200	191.50	349	7.304	13.5	98.9	313.24	0.56
L	1250	62.87	4796	15.863	6.3	99.3	318.41	0.47
M	1350	27.83	1100	59.458	1.7	98.7	322.55	0.67
N	1450	32.20	586	98.800	1.0	98.8	324.42	0.84
Sample CT06116 muscovite, staurolite zone (J=0.009173±0.000023)								
A	600	5.45	22	46.250	0.2	11.1	107.18	6.75
B	700	9.28	118	100.519	0.8	77.4	214.65	1.23
C	800	30.78	350	42.928	2.2	95.3	286.20	0.84
D	850	65.42	1008	34.444	2.8	96.1	292.34	0.65
E	900	190.47	2405	10.808	8.9	96.3	309.64	0.59
F	950	498.26	19922	3.461	28.6	99.1	311.50	0.34
G	1000	275.47	18882	6.322	15.7	99.2	301.06	0.42
H	1050	147.80	4544	13.540	7.3	98.3	295.72	0.47
I	1100	100.75	2275	18.318	5.4	98.0	304.69	1.04
J	1150	182.17	3175	12.029	8.2	98.4	298.74	0.61
K	1200	253.97	402	6.519	15.2	98.9	306.46	0.48
L	1250	59.89	980	24.146	4.1	99.0	312.13	0.65
M	1350	10.29	161	167.143	0.6	93.6	297.96	1.79
N	1450	4.04	34	667.143	0.1	93.4	306.23	5.44

Table 2

(continued)

Step	T°C	K/Ca	K/Cl	$^{40}Ar^{*}/^{39}Ar$	^{39}Ar (% total)	$\%^{40}Ar^{*}$	Age (Ma)	± Age
Sample JAW49A muscovite, chlorite zone (J=0.009168±0.000023)								
A	600	5.14	31	17.561	0.8	14.4	86.11	2.87
B	700	7.39	155	25.403	3.4	85.1	177.22	1.15
C	800	12.07	503	10.827	9.1	98.2	290.35	0.52
D	850	9.46	1196	11.163	8.9	98.9	305.28	0.61
E	900	6.69	1869	9.715	10.2	99.0	310.27	0.62
F	950	6.36	3606	7.744	12.8	99.2	317.85	0.49
G	1000	8.73	6715	6.529	15.2	99.3	323.81	0.58
H	1050	12.79	4768	7.807	12.7	99.3	323.78	0.49
I	1100	13.23	2639	8.294	12.0	99.2	318.03	0.53
J	1150	7.24	2216	7.635	13.0	99.1	327.87	0.60
K	1200	0.61	22	52.228	1.8	96.1	355.51	1.05
L	1250	0.08	45	512.222	0.2	92.2	654.01	8.08
Sample CT0713 muscovite, chlorite zone (J=0.009193±0.000023)								
A	600	8.13	39	25.882	0.7	17.6	88.64	2.64
B	700	17.19	206	29.732	3.0	88.9	200.79	0.55
C	800	50.73	608	12.893	7.6	98.5	288.06	0.48
D	850	69.06	2963	12.487	7.9	98.9	302.79	0.41
E	900	59.89	7344	9.593	10.3	99.0	303.99	0.40
F	950	76.95	**	6.942	14.3	99.2	312.56	0.54
G	1000	103.48	**	5.654	17.6	99.4	319.41	0.37
H	1050	89.44	26488	7.262	13.7	99.2	319.49	0.52
I	1100	62.27	6891	8.650	11.5	99.3	327.57	0.50
J	1150	33.74	4080	8.205	12.1	99.2	338.64	0.37
K	1200	2.11	20	77.500	1.2	89.9	354.59	1.12
L	1250	0.36	14	351.579	0.2	66.8	378.43	6.53
Sample CT0723 muscovite, chlorite zone (J=0.009184±0.000023)								
A	600	8.31	63	36.923	0.8	28.8	95.87	1.53
B	700	11.76	134	32.724	2.8	91.3	221.43	0.61
C	800	18.72	475	14.402	6.9	98.8	292.19	0.33
D	850	15.92	1316	13.244	7.5	99.2	302.59	0.39
E	900	12.76	2420	10.061	9.9	99.3	309.68	0.40
F	950	14.14	6848	7.448	13.4	99.5	313.95	0.43
G	1000	19.54	8254	5.324	18.7	99.5	316.91	0.43
H	1050	26.65	4231	5.312	18.7	99.5	320.58	0.44
I	1100	20.18	1687	9.698	10.3	99.4	321.69	0.36
J	1150	10.40	1188	14.006	7.0	98.6	325.34	0.47
K	1200	5.25	60	30.740	3.1	95.6	329.31	0.86
L	1250	1.10	51	141.803	0.6	86.5	325.38	1.79
M	1350	0.63	26	251.667	0.2	60.4	300.80	4.31
N	1450	0.84	44	493.529	0.2	83.9	338.72	6.85
Sample CT0705A amphibole, staurolite zone (J=0.009251±0.000023)								
A	700	0.18	11	110.946	0.7	82.1	1616.84	4.84
B	800	0.31	55	197.778	0.4	71.2	388.71	2.34
C	900	0.16	62	85.224	0.7	57.1	336.52	1.21
D	1000	0.07	109	24.212	3.1	75.3	371.19	0.90
E	1050	0.04	117	13.721	6.1	83.7	389.69	0.76
F	1075	0.05	158	13.879	6.5	89.8	397.52	0.71
G	1100	0.07	207	10.356	9.0	93.0	389.79	0.54
H	1125	0.08	268	6.556	14.5	95.2	381.78	0.45
I	1150	0.08	149	12.224	7.8	95.1	383.15	0.35
J	1175	0.09	149	13.268	7.2	95.4	387.48	0.41
K	1200	0.09	236	7.149	13.5	96.3	398.49	0.75
L	1225	0.09	237	8.993	10.8	97.3	402.15	0.37
M	1250	0.09	269	5.740	17.1	98.1	396.45	0.48
N	1450	0.07	211	35.830	2.7	97.1	411.20	0.79

be ~375 Ma which is consistent with the time of regional peak metamorphism at 380 Ma (Lancaster and others, 2008). The maximum age of 393 Ma from a fourth sample, CT0714 (fig. 7B), is also consistent with these ages.

Table 2

(continued)

Step	T°C	K/Ca	K/Cl	$^{40}Ar^*/^{39}Ar$	^{39}Ar (% total)	$\%^{40}Ar^*$	Age (Ma)	± Age
Sample CT0718A amphibole, staurolite zone (J=0.009238±0.000023)								
A	700	0.17	30	21.667	3.7	79.3	815.35	1.24
B	800	0.66	130	66.691	1.4	90.7	428.26	1.47
C	900	0.66	125	21.439	4.0	86.4	545.54	1.07
D	1000	0.12	156	8.791	9.4	82.9	344.85	0.55
E	1050	0.04	101	15.310	5.8	88.8	406.43	0.82
F	1075	0.04	77	19.663	4.5	87.5	454.43	0.87
G	1100	0.03	69	17.975	4.9	87.9	523.15	0.82
H	1125	0.03	79	4.609	20.9	96.2	507.76	0.65
I	1150	0.03	21	45.598	1.8	83.9	396.50	1.47
J	1175	0.03	46	25.099	3.5	88.6	424.01	0.79
K	1200	0.03	69	7.654	11.7	89.7	460.08	0.56
L	1225	0.03	67	5.359	17.4	93.3	522.20	0.62
M	1250	0.03	75	10.437	8.9	93.1	480.58	0.59
N	1450	0.03	72	43.810	2.1	92.0	446.84	1.18

** Cl derived ^{38}Ar below detection limit.

Muscovite.—The interpretation of the muscovite age spectra follows the thorough discussion of Kunk and others (2005) and is guided by the observation of at least two generations of muscovite-bearing fabrics in the matrix of all samples dated. Muscovite intergrown and forming fabrics with biotite is overprinted and cross cut by fabrics defined by muscovite + chlorite intergrowths (for example, fig. 3). The muscovite-biotite fabrics are texturally older than the muscovite-chlorite fabrics. It was impossible to physically separate and isolate muscovite from different fabric-forming generations for argon dating analysis; consequently, the muscovite mineral separates all contained grains from both mica age populations. The closure temperature for argon diffusion in muscovites is ~350 °C ± 50 °C (Jäger, 1979; Mcdougall and Harrison, 1999) which overlaps with the temperature of the biotite isograd in the Wepawaug Schist (~400 °C, Ague, 1994b). Muscovite intergrown with biotite occurs only in biotite zone and higher-grade samples and so must have experienced temperatures in excess of 350 °C. Muscovite from texturally older muscovite-biotite intergrowths will, therefore, yield cooling ages. Muscovite intergrown only with chlorite could not have experienced biotite-zone, or higher, metamorphic conditions and probably did not exceed ~350 °C; therefore, muscovite from texturally younger muscovite-chlorite intergrowths will likely yield crystallization ages. The resulting muscovite age spectra should reflect multiple generations of muscovite growth where the older ages on the spectra may reflect a minimum cooling age of muscovite-biotite fabrics and the younger ages on the spectra may reflect a maximum below-closure crystallization age of younger muscovites (for example, figs. 8C-8L). The older age is a minimum age because it is mixed with muscovite from the younger age population and, likewise, the younger age represents a maximum age because it is mixed with muscovite from the older age population. The two chlorite-zone samples (figs. 8A and 8B) are an exception to this general interpretation. They were collected in chlorite-zone rocks, have no biotite in them, and likely never exceeded the closure temperature for argon diffusion in muscovite. Thus in these rocks, all the muscovite in all cleavage generations must yield crystallization ages albeit from multiple orogenic events.

The effects of mineral impurities and ^{39}Ar recoil are apparent in some of the muscovite age spectra, commonly affecting the results of both the highest and lowest temperature heating steps. Apatite inclusions, in particular, are commonly identified

TABLE 3

Ar Cooling and crystallization ages of minerals in rocks of the Orange-Milford complex and surroundings

Field Number (Fig. 1)	Mineral	Rock Type	Easting	Northing	Cooling Age (Ma)	Growth Age (Ma)	Comment
Orange-Milford Belt - Chlorite zone							
CT0723	Muscovite	chl-mu phyllonite	666378	4568246	329	292	
CT0713	Muscovite	chl-mu phyllonite	666117	4571413	339	288	
Orange-Milford Belt - Biotite zone							
CT0701A	Muscovite	mu-grt schist	664918	4574298	343	281	
CT0701B	Muscovite	mu-grt schist	664918	4574298	347	292	
CT0708	Muscovite	mu schist			350	312	
JAW49A	Muscovite	mu-grt schist			329	290	
Orange-Milford Belt -Staurolite zone, east of EDSZ							
CT0726	Amphibole	amphibolite	660733	4565611	377	–	plateau age, correlates at 377±2 Ma
CT0714	Amphibole	amphibolite lens	662071	4573502	393	–	maximum cooling age
CT0718	Amphibole	amphibolite	662502	4569521	–	–	uninterpretable results
CT06116	Muscovite	mu-chl schist	658427	4566195	312	296	
CT0715	Muscovite	mu-grt schist	662049	4572893	339	320	
CT0714B	Muscovite	mu-bt schist	662071	4573502	335	324	
JAW35A	Muscovite	mu-bt schist			355	311	
Connecticut Valley Synclinorium (CV S) -Staurolite zone, west of EDSZ							
CT0703	Muscovite	granite pegmatite	656742	4577936	349	343	
CT0706	Muscovite	mu-bt-grt schist	658358	4573432	324	302	
CT0705	Amphibole	amphibolite	658588	4574485	374	–	correlation age
CT0712	Amphibole	bt-amphibolite	668481	4587815	375	–	plateau age, correlates at 375±3 Ma

by unacceptably low K/Ca ratios (denoted * fig. 8). Recoil occurs due to the enrichment of ^{39}Ar in chlorite grains intergrown with muscovite and the resulting depletion of ^{39}Ar in the muscovite following irradiation of the samples. Electron microprobe analysis (for example, fig. 4D) and BSE imaging (for example, fig. 3) demonstrate that chlorite is intimately intergrown with muscovite at the μm-scale throughout the Orange-Milford belt. Composite muscovite-chlorite flakes are typically present in mineral separates making it impossible to completely separate all chlorite from the muscovite samples. Hence contained recoil effects are expected in the age spectra. Recoil, discussed in detail by Kunk and others (2005) and Wintsch and others (2010), commonly affects the youngest age steps on the muscovite spectra of some samples. Recoil is recognized by the rise-fall-rise pattern of ages on some of the age spectra (denoted with "recoil," figs. 8H-8L). All muscovite separates produced generally climbing or sigmoidal age spectra; no plateaus were produced and no absolute ages can be interpreted (fig. 8). Inverse isotope correlation is not an appropriate tool to reduce the data from these samples because they contain more than one age population.

Excess argon can disrupt expected age spectra patterns but the contributions of excess argon affect each age spectrum to a different extent. There is no expected correlation between the amount of excess argon in a sample and the deviation of its age spectrum from a normal plateau. In the case of the muscovite age spectra reported here, all samples showed older ages that converge towards ~360 Ma and younger ages that converge towards ~280 Ma (fig. 9). This degree of agreement among samples would not be expected, and would be highly improbable, if the presence of excess argon was responsible for the climbing age spectra patterns in these samples.

Orange-Milford belt, chlorite zone.—Samples CT0723 and CT0713 are chlorite-muscovite phyllites characterized by crosscutting fabric generations all defined by chlorite and muscovite (figs. 3I-3L). These two samples yeild climbing age spectra (figs. 8A and 8B). The spectrum for sample CT0723 (fig. 8A) climbs from an age of 292 Ma to an age of 329 Ma. The spectrum for sample CT0713 (fig. 8B) climbs from an age of 288 Ma to an age of 339 Ma. The K/Ca ratios suggest that the spectra of both samples are affected by impurities in the highest- and lowest-temperature steps (*, figs. 8A and 8B).

Orange-Milford belt, biotite-garnet zone.—Samples CT0701A and B, CT0708, and JAW49A are muscovite-biotite-garnet schists that include well-developed muscovite + chlorite overprinting fabrics (for example, figs. 3E-3H). Similar to the chlorite-zone samples, the K/Ca ratios suggest that the lowest and highest temperature steps for both of these samples are associated with impurities in the mineral separates (*, figs. 8C-8E). Samples CT0701A and CT0701B are two separate samples collected at one site and the mineral separates chosen for analyses were of different size fractions. Muscovites from samples CT0701A were between 125 to 150 μm, those from sample CT0701B were 150 to 180 μm. The spectrum for CT0701A (fig. 8C) climbs from an age of 281 Ma to 343 Ma, whereas the spectrum for CT0701B (fig. 8D) climbs from an age of 292 Ma to 347 Ma. The size fraction chosen for argon dating analysis for these rocks had little affect on the age results. Similar age spectra also suggest that muscovites defining texturally distinct fabrics are comparable in size. The age spectrum for sample CT0708 (fig. 8E) climbs from an age of 312 Ma to an age of 350 Ma and the age spectrum of sample JAW49A (fig. 8F) climbs from an age of 290 Ma to an age of 329 Ma.

Orange-Milford belt, staurolite/kyanite zone.—Samples JAW35A, CT0714B, CT06116, and CT0715 (figs. 8G-8J, table 2) are muscovite schists containing abundant garnet and staurolite porphyroblasts and dominant muscovite + biotite fabrics. These fabrics are cut by texturally younger muscovite + chlorite fabrics that are not equally developed yet are present in all samples. The climbing age spectra for these higher-

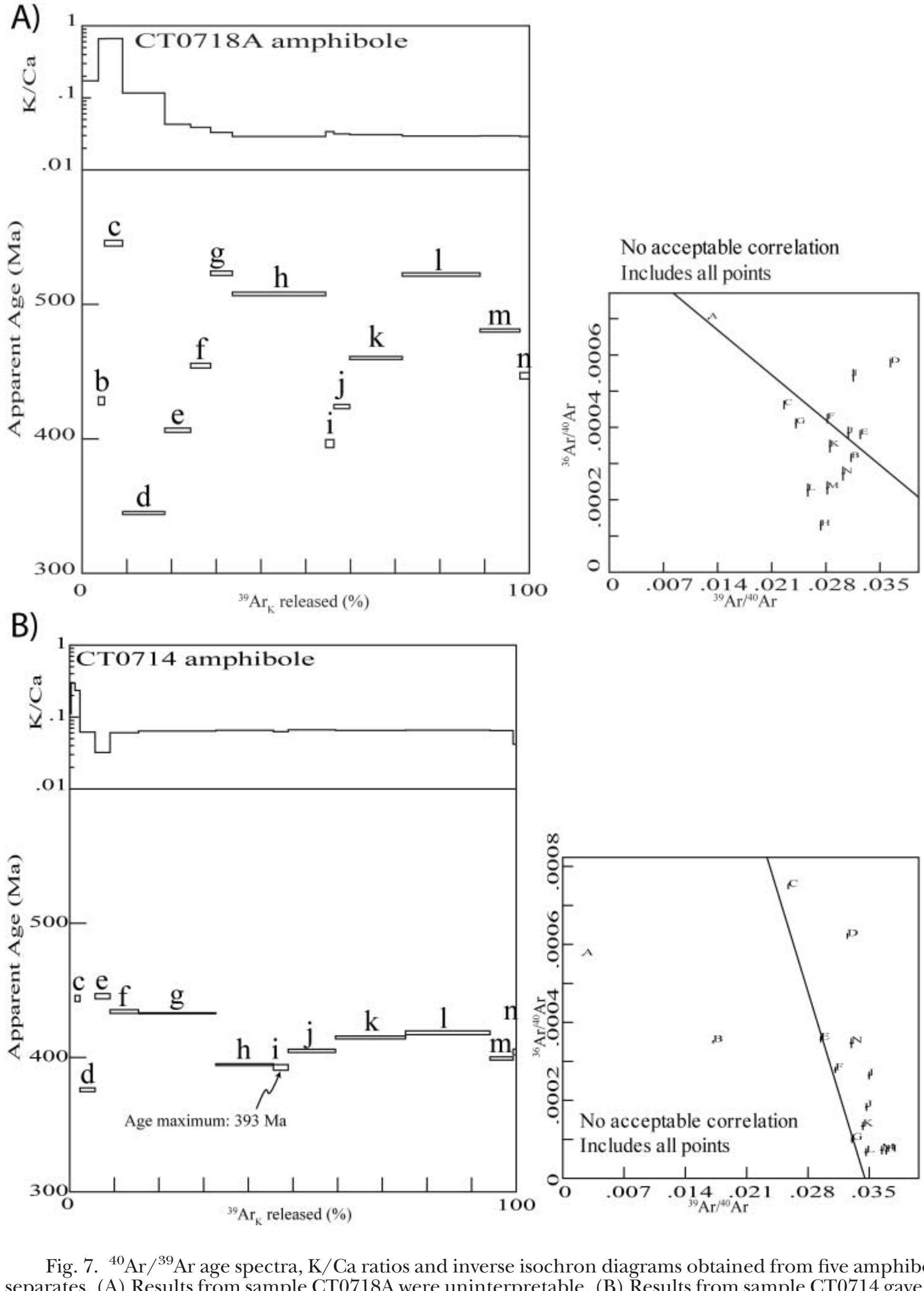

Fig. 7. $^{40}Ar/^{39}Ar$ age spectra, K/Ca ratios and inverse isochron diagrams obtained from five amphibole separates. (A) Results from sample CT0718A were uninterpretable. (B) Results from sample CT0714 gave an age maximum of 393 Ma but there was no correlation on the isochron diagram. (C) Sample CT0705A gave an isochron age of 374 ± 4 Ma over steps F–J. (D) A plateau age of 377 ± 1 Ma over steps E–G in sample CT0726 was reproduced by an isochron age of 377 ± 2 Ma for steps D–H. (E) A plateau age of 375 ± 1 Ma over steps E–H in sample CT0712 was reproduced by an isochron age of 375 ± 3 Ma for steps E–J.

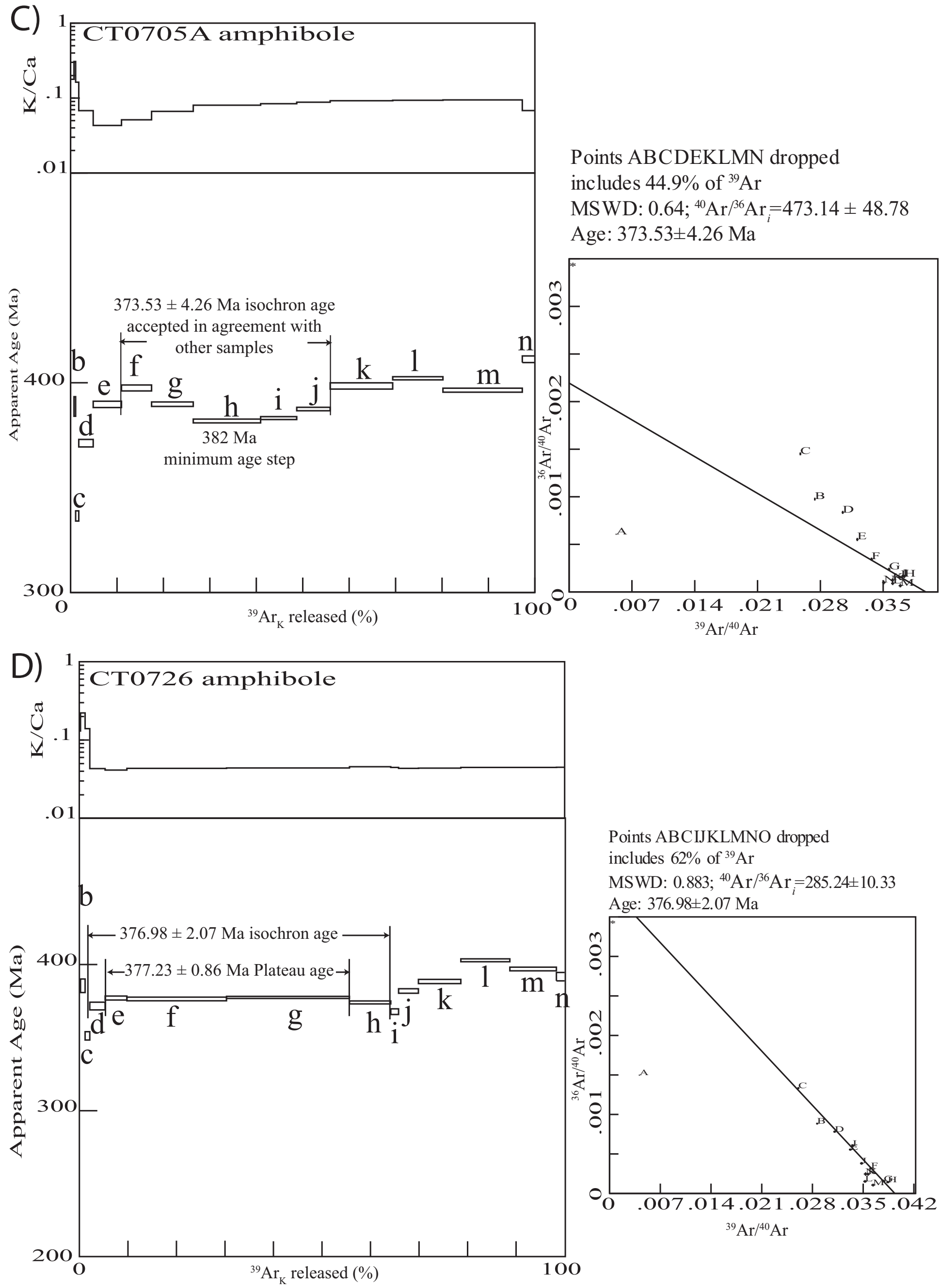

Fig. 7 (continued).

grade samples show the effects of recoil to a higher degree than do the age spectra from lower-grade rocks. This may be due to the finer grain-size and extent of

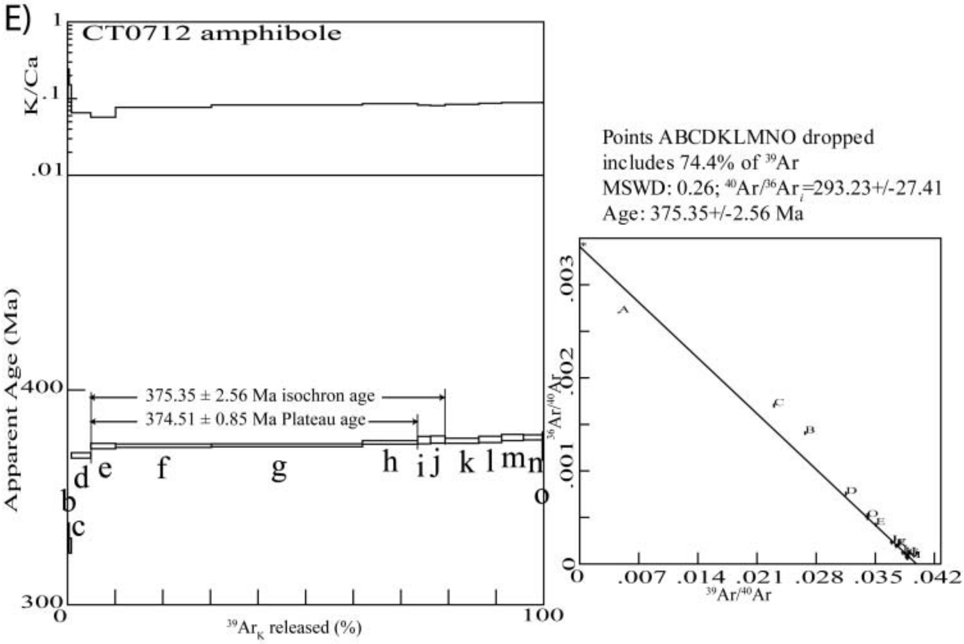

Fig. 7 (continued).

intergrowth of chlorite with muscovite in the texturally younger overprinting fabrics in these rocks. Sample JAW35A (fig. 8G) yields an age spectrum that climbs from 311 Ma to an age of 355 Ma. The age spectrum for sample CT6116 (fig. 8H) climbs from an age of 296 Ma to an age of only 312 Ma. Sample CT0714B (fig. 8I) yields an age spectrum that climbs from 324 Ma to 335 Ma. Finally, the age spectrum for sample CT0715 (fig. 8J) climbs from 320 Ma to 339 Ma. These age spectra and the associated K/Ca ratios show evidence for inclusions or impurities in the highest-temperature age steps (*, fig. 8G-8J).

Rowe-Hawley belt, staurolite/kyanite zone.—Samples CT0703 and CT0706 were collected west of the East Derby shear zone from a deformed granitic pegmatite and coarse-grained muscovite-biotite schist, respectively. Texturally late chlorite + muscovite fabrics are present and both age spectra, and the associated K/Ca ratios, show the effects of recoil due to fine-grained chlorite-muscovite intergrowths (figs. 8K and 8L). The part of the spectrum for sample CT0703A unaffected by recoil (fig. 8K) barely climbs from 343 Ma to 349 Ma whereas that for sample CT0706 (fig. 8L) climbs from 302 Ma to 324 Ma.

DISCUSSION

In the above sections, details of textures and fabrics are described together with the results of $^{40}Ar/^{39}Ar$ dating of mica separates. We document texturally prograde fabrics overprinted to variable degrees by a younger, universally cross-cutting fabric. The younger fabric is composed of muscovite ± chlorite, whereas the older fabric is composed of muscovite + chlorite in chlorite-grade samples and muscovite + biotite in biotite- and higher-grade samples. These observations suggest that the younger muscovite-chlorite fabric is retrograde. We also present seventeen amphibole and white-mica age spectra for samples distributed across the metamorphic gradient. The

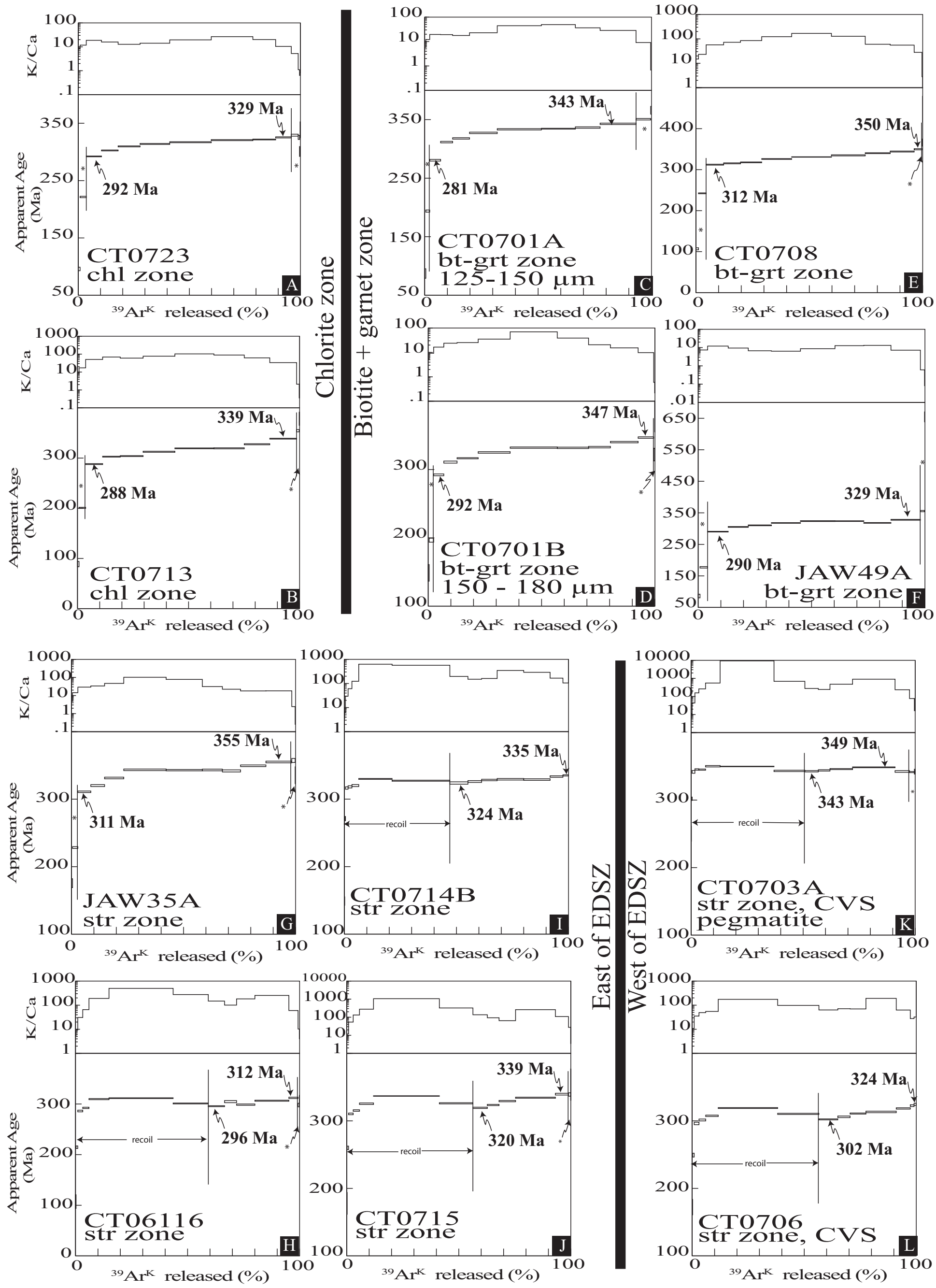

Fig. 8. $^{40}Ar/^{39}Ar$ age spectra and K/Ca ratios obtained from twelve muscovite separates organized from low- to high-grade. Asterisks indicate steps not deemed reliable due to impurities or ^{39}Ar loss. All samples produced climbing spectra and half (plots H-L) are significantly affected by recoil.

results of the argon thermochronology for the OMB show ubiquitous climbing muscovite age spectra (for example, fig. 9) and uniform amphibole plateau and/or correlation ages (for example, figs. 7D and 7E).

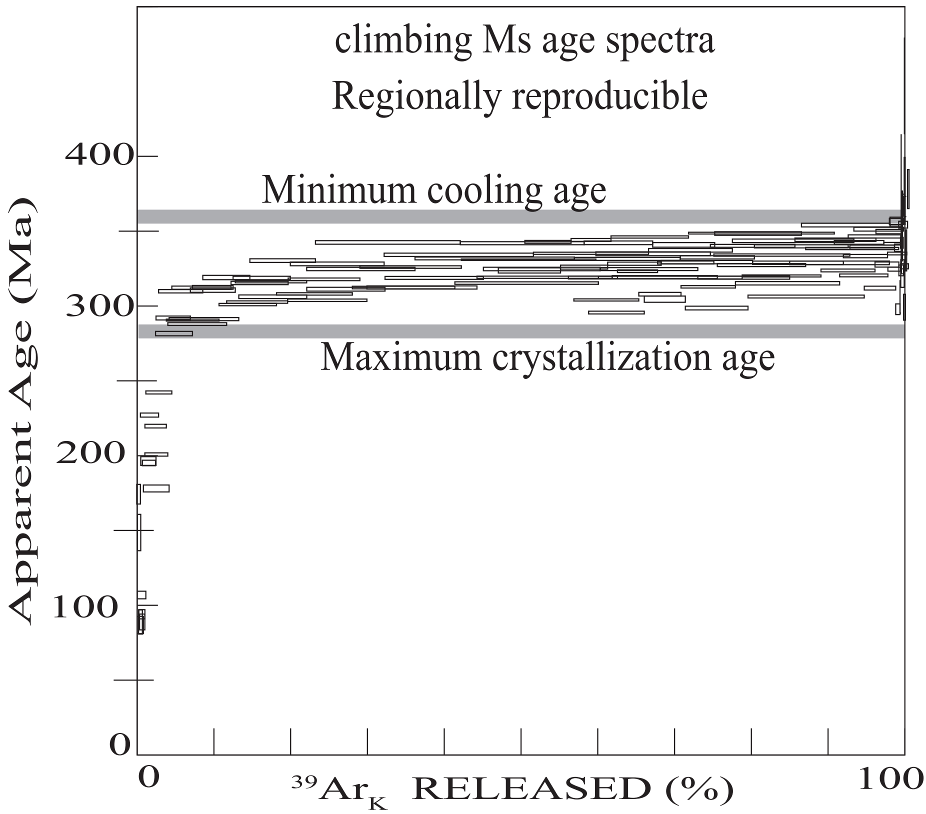

Fig. 9. Compiled $^{40}Ar/^{39}Ar$ age spectra for all 12 muscovite samples showing regional reproducibility of climbing ages from a maximum crystallization age of ~280 Ma to a minimum cooling age of ~360 Ma. Steps affected by recoil are not shown in several spectra.

Retrograde Overprint Evident in Argon Results

The pervasive Alleghanian overprint on prograde Acadian fabrics is evident in climbing muscovite age spectra that tail up in the high-temperature steps to a maximum age of ~360 Ma (fig. 9, tables 2 and 3). The climbing muscovite age spectra reported here are interpreted to reflect the presence of several generations of muscovite observed petrographically in these rocks (table 3, fig. 9). All prograde muscovite that grew in rocks at or above biotite-grade crystallized at temperatures greater than ~400 °C (Ague, 1994b). This muscovite yields a common cooling age consistent with the time at which the rocks cooled through ~350 °C. For these rocks, the cooling age appears to be ≥360 Ma (fig. 9), consistent with cooling from an Acadian metamorphic event. It follows that any muscovite that crystallized later than ~360 Ma must have crystallized below the closure temperature for Ar-diffusion in muscovite and will yield a second, younger, muscovite crystallization age indicative of the time at which retrograde muscovite grew in these rocks. This younger age, ≤280 Ma is approached by the low temperature steps of the muscovite age spectra (fig. 9, tables 2 and 3) and is consistent with an Alleghanian crystallization event. Back-scattered electron (BSE) petrography reveals the presence of a pervasive muscovite-chlorite fabric that cuts all earlier fabrics in these rocks [for example, S(al), fig. 3]. The maximum and minimum apparent ages of the individual climbing spectra reflect the

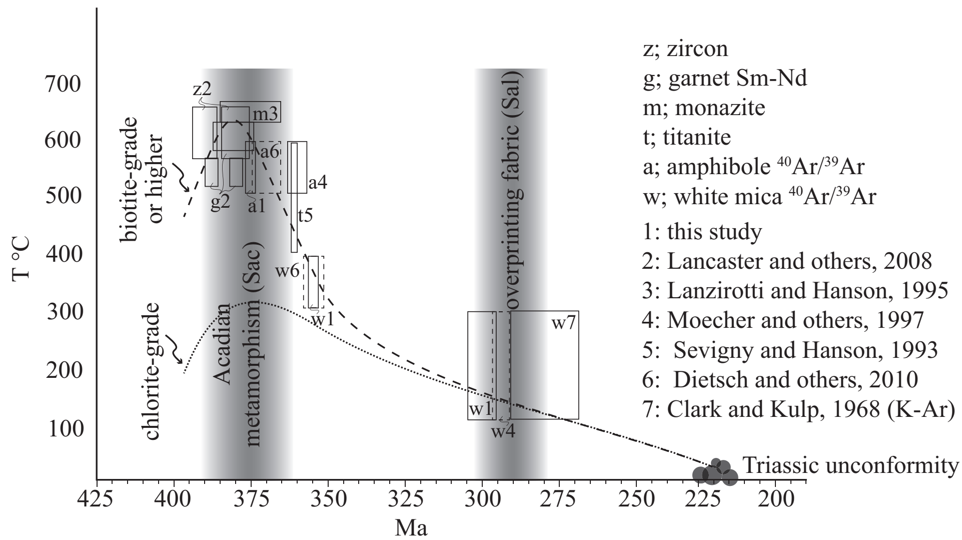

Fig. 10. Temperature-time diagram for the Orange-Milford belt. Smooth curved lines represent crustal levels metamorphosed to biotite and higher (long dashed) and chlorite (short dashed) grades during the Acadian. Amphibole and muscovite cooling ages constrain the cooling rate following Acadian metamorphism. Early Permian ages reflect Alleghanian recrystallization at greenschist facies. All rocks now exposed at the surface were covered by Triassic Hartford basin sediments, ~225 Ma (small cluster of circles). Rectangular boxes include estimated errors.

proportion of muscovite populations with cooling ages versus crystallization ages in those separates. Samples that contain a highly penetrative late muscovite-chlorite fabric will be weighted more toward Alleghanian crystallization ages (for example, samples CT0723, CT0713, JAW49A, figs. 8A, 8B, and 8F) and samples with a less penetrative late muscovite-chlorite cleavages will be weighted toward the Acadian cooling ages (for example, samples CT0714B, CT0715, CT0703A, figs. 8I-8K). Although the temperatures at which these distinct fabrics grew cannot be precisely established, the argon age spectra consistently reflect the presence of a younger age population (~280 Ma). This younger age confirms that this late fabric grew below closure during a Permain retrograde fabric-forming event.

Acadian Versus Alleghanian Fabrics

Acadian metamorphic assemblages and fabrics are well known and well-preserved in much of western Connecticut (for example, Lancaster and others, 2008; Dietsch and others, 2010). Pressure-temperature data from the Wepawaug Schist (for example, Ague, 1994b) document a metamorphic field gradient from chlorite- to kyanite-/staurolite-grade conditions, and Lancaster and others (2008) report Sm/Nd garnet ages documenting garnet growth in the Wepawaug Schist at ~380 Ma. Additional regional geochronological results document monazite and sphene participating in defining metamorphic fabrics and suggest a middle Devonian amphibolite-facies metamorphic event (Sevigny and Hanson, 1993; Lanzirotti and Hanson, 1995, 1996). K-Ar cooling ages from the OMB and adjacent Rowe-Hawley zone suggest late Paleozoic cooling following this middle Devonian regional metamorphism (Clark and Kulp, 1968). Amphibole ages from the OMB reported here are consistent with these regional studies and suggest cooling from regional metamorphic temperatures through 500 °C at ~375 Ma (fig. 10). These ages are consistent with and confirmed by the work of Dietsch and others (2010) who report amphibole ages in the range of 365 to 375 Ma for the Waterbury Dome.

Moecher and others (1997) also present amphibole $^{40}Ar/^{39}Ar$ ages produced by the step heating method. They reported plateau or total fusion ages for amphibole-bearing samples. The minimum age of sample 1 (M1, fig. 1B) with an acceptable radiogenic yield >95 percent is 361 Ma, but one step with a radiogenic yield of only 91 percent produces an age of 339 ± 9 Ma. All the other samples, including M2 (fig. 1B) produce Carboniferous amphibole ages. These are younger than any of the amphibole ages found in this study but we do not consider these results necessarily in conflict. Matthews and Wintsch (2008) identified an increasing metamorphic field gradient and a decreasing cooling age gradient approaching the EDSZ from the west and propose that the SE margin of the Rowe-Hawley belt was tilted by motion along this fault. In fact, a field gradient in cooling ages requires tilting to be younger than the youngest age of in the tilted section. Thus the ages reported by Moecher and others (1997) may be expected not to coincide with the ~375 Ma ages we report.

Muscovite ages at the high-temperature end of sigmoidal age spectra reported here from the Wepawaug Schist suggest a regional minimum cooling age of ~360 Ma. The ages of muscovite reported by Dietsch and others (2010) for the rocks mantling the Waterbury dome lie between 351 to 363 Ma. They do not report extensive overprinting textures so we take these results to support our interpretation that 360 Ma is a reasonable estimate of the cooling age of white mica from regional Acadian metamorphism. Moecher and others (1997) report mostly Permian and late Pennsylvanian white mica ages, only one of these samples lies east of the EDSZ (M6, fig. 1B). Moecher and others (1997) report minimum ages from sigmoidal age spectra that are younger than the late Devonian age reflective of cooling from Acadian metamorphism and describe multiple, overprinting foliations in many of their dated samples. Thus, we consider these results consistent with ours in that many steps in the age spectra reflect a mixture of a Devonian cooling age and a younger crystallization age. Young ages in the East Derby shear zone are also reported by Clark and Kulp (1968). These regional geochronological results are compiled with ours on a temperature-time diagram (fig. 10) and collectively confirm a robust Acadian metamorphic event followed by a younger low-grade recrystallization event.

Telescoping of Isograds

A metamorphic field gradient of deeper, higher-grade rocks in the northwest and shallower, lower-grade rocks in the southeast is exposed in the Orange-Milford belt. Tilting up to the northwest must have occurred after the rocks reached retrograde greenschist facies conditions following Acadian metamorphism to expose this field metamorphic gradient. Tilting prior to 360 Ma, when the rocks were still warm, would have reset the Acadian isograds parallel to the paleo-surface. The metamorphic grade in the Wepawaug Schist increases from chlorite grade to staurolite-kyanite grade over approximately 4 kilometers (Fritts, 1965a). Specifically, the distance between the biotite-garnet and staurolite-kyanite isograds varies between 2.5 to 4 km. The temperatures of formation of the biotite and staurolite isograds are taken as ~400 °C and ~550 °C, respectively (Ague, 1994b) which corresponds to a separation of ~8 km given the *ca.* 19 °C/km geothermal gradient documented for these rocks during peak metamorphism (Ague, 2002). The map distance of 4 km between isograds yields an apparent field geothermal gradient of ~38 °C/km. Thermobarometry for rocks from this area (Ague, 2002) indicate that pressures change by 3 kbars over a 6 km map distance in the field and yield an apparent 50 MPa/km geobaric gradient. A 50 MPa/km geobaric gradient requires an average rock density of 5 g/cm^3, which is not possible. For a rock density of ~2.65 g/cm^3, a reasonable density for continental crustal material, the lithostatic pressure gradient established during metamorphism should be no greater than 25 MPa/km and a 3 kbar change in pressure must be accomplished over ~12 km of structural relief. Thus the apparent doubling of the lithostatic pressure gradient and shortening of the distance between the isograds in the Wepawaug Schist cannot have been accomplished by simple tilting of the rocks. The isograd spacing in the Wepawaug Schist must have been physically reduced by at least 50 percent of their original separation after they were established.

Several possibilities exist for this telescoping of the isograds. It is possible that thrust faults could juxtapose lower-grade rocks against higher-grade rocks. This could produce the appropriate amount of shortening but the presence of such faults has not been documented despite quadrangle-scale mapping (Fritts, 1965a) and other field studies (Ague, 1994a; Lanzirotti and Hanson, 1996). A thrust fault should also be discernable in the P-T data as a substantial discontinuity in field P-T gradient. The P-T estimates for this area (Ague, 2002) fall along a linear trend and do not show any evidence for the existence of a km-scale fault. Thus, discrete faulting is not likely to be the cause of the compressed isograd spacing.

An alternate explanation for the collapsed isograd spacing is telescoping and thinning of the rocks containing the isograds. In this case, telescoping, like tilting, must have occurred after all the rocks had reached lower greenschist facies conditions to preserve the apparently uniform Acadian cooling ages. A conceptual end-member model of the OMB as a northeast-trending rectangular prism comprised of infinitesimally thin rectangular slices oriented NNE within the prism (fig. 11A) is used to explore the effects of dextral shearing as a means of regional thinning. The boundaries of each thin slice operate as discrete strike-slip shear zones so that each slice can slip along a northeast-southwest trajectory. An E-NE-oriented σ_1 acting on a resistant NE-striking body partitions into SW-directed shear stress and W-directed compressional (normal) stress (fig. 11A). Each thin rectangular slice will theoretically shear against its neighbors such that the western border of the slice slips toward the southwest with respect to the adjacent slice (fig. 11B). Northeast trending marker lines, mimicking the biotite and staurolite isograds and cutting across shear boundaries within the prism, converge as shearing progresses (fig. 11B). Continued dextral simple shearing is thus capable of stretching the Orange-Milford belt along a NE-SW axis, resulting in broadly distributed strain including recrystallization of metamorphic fabrics and telescoping of the Acadian isograds by roughly fifty percent.

Field observations associated with this study identified garnet, staurolite, and K-feldspar porphyroblasts in the high-grade Wepawaug Schist and Pumpkin Ground orthogneiss with asymmetric delta-type tails (Growdon and others, 2006). Asymmetric dextrally offset drag folds (for example, fig. 2A) and quartz veins (for example, fig. 2B) and granitic dikes that cut foliations were subsequently extended and rotated into near parallelism with these same foliations. Indeed, up to four mapped foliations (Fritts, 1965a; Ague, 2005; Bell and Newman, 2006) in the field are all rotated into subparallelism with each other and many foliations contain SW-plunging mineral lineations (Growdon and others, 2006). These observations are strong evidence for pervasive greenschist facies dextral shearing and transpression. Thinning was at least partially accomplished by pressure solution and crenulation of earlier cleavages (figs. 3 and 4; see also Bell and Newman, 2006). Over time this dextral shearing would rotate the isograds into near-parallelism with boundaries of zones of localized strain, such as the EDSZ. In fact, abundant evidence for a late Paleozoic dextral tectonic regime is well documented throughout the New England and Maritime Canada Appalachians (Hoffman, 1988; Swanson, 1992; St. Peter, 1993; Pe-Piper and Piper, 2004; Simancas and others, 2005; Wang and others, 2006; Gerbi and West, 2007; Waldron and others, 2010). The regionally pervasive muscovite crystallization ages show that in the Wepawaug Schist this shearing occurred in the Early Permian.

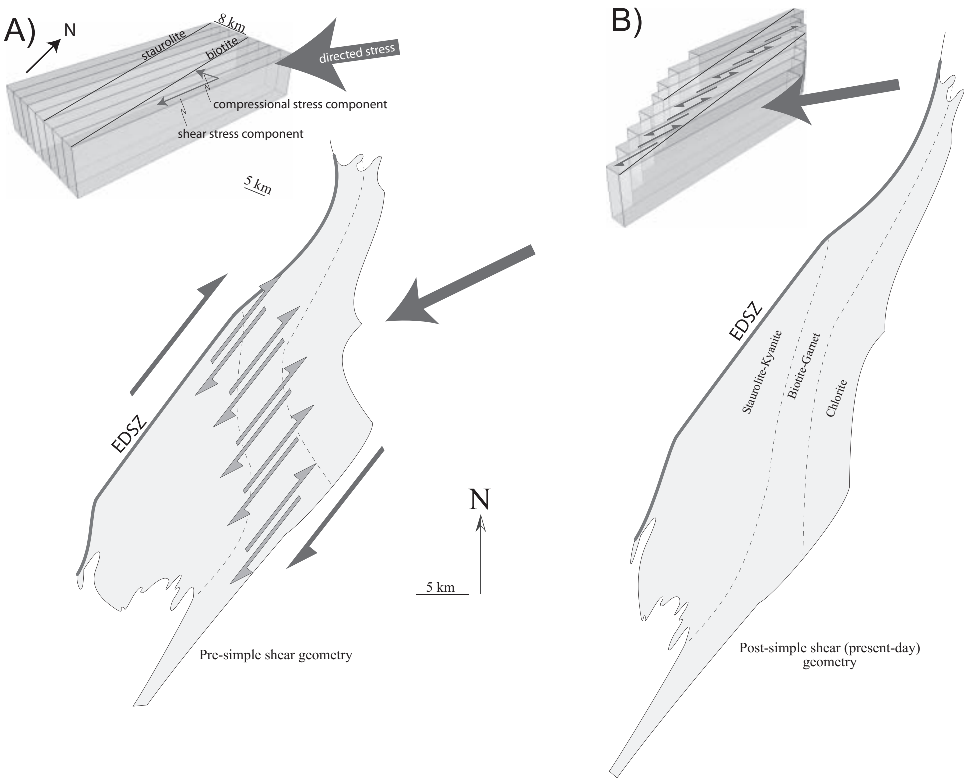

Fig. 11. Sketches of theoretically modeled isograd compression due to simple shear in the Wepawaug Schist. (A) Theoretical rectangle composed of thin slices with isograds spaced 8 km apart on the surface and accompanying retro-deformed Wepwawaug Schist with Acadian isograds. (B) Theoretical rectangle resulting from strike-slip simple shearing along the boundaries of each thin slice and accompanying present-day geometry of the Wepawaug Schist with isograds compressed to at least 50% of their original spacing.

Tectonic Speculations

At the beginning of the Paleozoic the eastern margin of Laurentia was probably defined by the rifts and transform faults inherited from the Neoproterozoic opening of the Iapetus Ocean (Wilson, 1966; Rankin, 1976; Thomas, 2006). The saw-tooth pattern of the margin (fig. 1A) established a series of promontories and recesses that would have strongly influenced the distribution and intensity of subsequent deformation along this margin. Crustal rocks forming promontories would experience relatively high strain and record more complex poly-metatmorphism and poly-deformation whereas recesses would contain rocks with relatively low strain and potentially simpler structural and metamorphic histories. In the central Appalachians, the Pennsylvania recess (fig. 1A) sequesters rocks deformed in the Silurian and sheltered them from further deformation during the Acadian or Alleghanian (Wintsch and others, 2010). In contrast, the New York promontory (fig. 1A) would have been well positioned to receive repeated deformations during multiple Paleozoic accretionary events giving rise to overprinting metamorphic assemblages and structural fabrics. By the late Paleozoic these rocks would have been cold (for example, Roden-Tice and Wintsch, 2002; Dietsch and others, 2010). Their high feldspar contents would have made them strong relative to the overlying schists (for example, Shea and Kronenberg, 1993), and relative to the rocks to the east still under anatectic conditions (Wintsch and others,

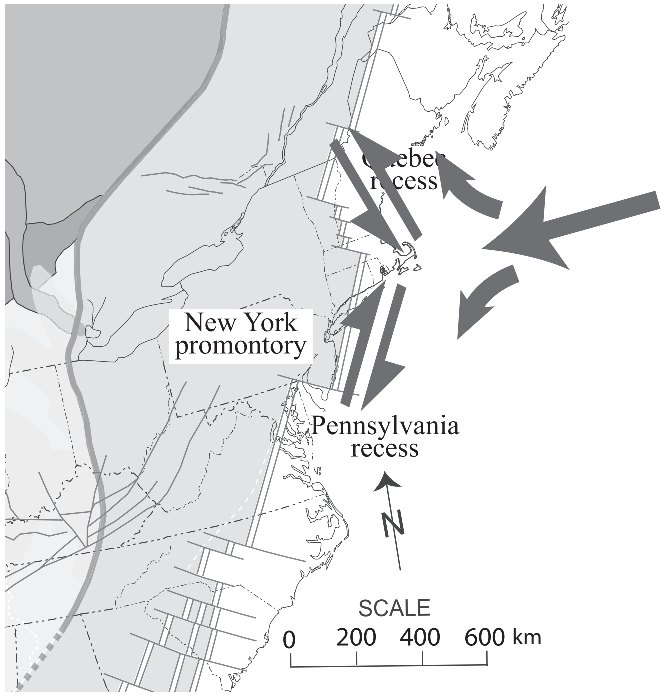

Fig. 12. Model for Alleghanian escape tectonics along the New York Promontory showing the approach of Gondwanaland in the late Paleozoic causing extrusion of rocks of the Connecticut Valley series into the Pennsylvania and Quebec recesses.

2003). Thus the promontory would have acted as a buttress against the accreting terranes as Gondwana approached.

In a regional context, the Wepawaug Schist shares many petrographic, structural, and tectonic characteristics documented in the Waits River and Northfield Formations in Vermont. This similarity is strong enough that Fritts (1962) correlated the two sequences, a correlation endorsed by Rodgers (1970). In addition to the lithostratigraphic similarities, the Middle to Late Devonian age of metamorphism, and Permian age of fabric overprinting of the Wepawaug Schist found here (see also Lancaster and others, 2008) is indistinguishable from that found in Vermont near the Westminster West fault (McWilliams and others, 2005; McWilliams, ms, 2008). Whereas the stratigraphic and metamorphic similarities are striking, the structures are antithetic. The kinematic indicators in the Wepawaug Schist all show strong dextral motion, whereas the Westminster West fault zone shows sinistral motion (Armstrong and others, 1997; Ratcliffe and others, 2011; Walsh and others, 2012), also in the early Permian (McWilliams and others, 2013). The apparently contradictory kinematics can be reconciled by noting that southern Connecticut and Vermont are separated by the New York promontory. In this case, the approach of Gondwanaland from the east (present coordinates) in the late Paleozoic (Hatcher, 2005) could easily led to escape tectonics. The relatively weak mica-rich sediments would have been extruded along the Laurentian buttress toward the northern Quebec and southern Pennsylvanian recesses (fig. 12). Such a model acknowledges the strength of the cold Laurentian buttress, explains the locus of strain along the East Derby shear zone, and accounts for the synchronicity of the deformation as well as the opposing kinematics within the lithologically similar Waits River and Northfield Formations and the Wepawaug Schist.

CONCLUSIONS

We have identified a retrograde schistosity throughout the Wepawaug Schist of the Orange-Milford belt, southwestern Connecticut that is regionally pervasive and locally penetrative (East Derby Shear Zone). The folia are uniformly defined by muscovite + chlorite in rocks ranging from chlorite to staurolite-kyanite grade. $^{40}Ar/^{39}Ar$ age spectra of white micas in these samples produce patterns that climb from ~280 Ma to ~360 Ma. These spectra are interpreted to reflect mixtures of two populations of mica: a younger retrograde cleavage younger than 280 Ma and an older population cooling ~360 Ma. Cooling ages of four amphibole separates from amphibolite-facies rocks corroborate other regional evidence for cooling at ~375 Ma from an Acadian metamorphic event. The younger cleavage suggests retrograde deformation, likely associated with crustal thinning, during the Alleghanian.

ACKNOWLEDGMENTS

We thank Laura Jones and Brooks Proctor for help with field work and the Calhoun family in Bethany, Connecticut for providing a home away from home during the field season, and Drs. Chusi Li and Juergen Scheiber for help with EMP and SEM analyses at Indiana University. We are grateful to Ryan McAleer, Dr. Cory McWilliams, Dr. Rebecca Stokes, and Miriam Attenoukon for helpful discussions. This work benefited greatly from constructive reviews by Drs. Dyk Eusden, Chris Hepburn, and Penelope Lancaster and discussions with and input from Dr. Jay Ague. We are especially grateful for access to samples JAW35A and JAW49A, for his help with field locations, his expertise in the field area, his organization of field trips to crucial outcrops in the field area, and for helpful discussions about this research. We acknowledge partial support from NSF grant EAR-9909410 and EAR-0510857 to Wintsch and Dorais, and from the Indiana University Department of Geological Sciences.

References

Ague, J. J., 1994a, Mass transfer during Barrovian metamorphism of pelites, south-central Connecticut; I, Evidence for changes in composition and volume: American Journal of Science, v. 294, n. 8, p. 989–1057, http://dx.doi.org/10.2475/ajs.294.8.989

——— 1994b, Mass transfer during Barrovian metamorphism of pelites, south-central Connecticut. II: Channelized fluid flow and the growth of staurolite and kyanite: American Journal of Science, v. 294, n. 9, p. 1061–1134, http://dx.doi.org/10.2475/ajs.294.9.1061

——— 2000, Release of CO_2 from carbonate rocks during regional metamorphism of lithologically heterogeneous crust: Geology, v. 28, n. 12, p. 1123–1126, http://dx.doi.org/10.1130/0091-7613(2000)28⟨1123:ROCFCR⟩2.0.CO;2

——— 2002, Gradients in fluid composition across metacarbonate layers of the Wepawaug Schist, Connecticut, USA: Contributions to Mineralogy and Petrology, v. 143, n. 1, p. 38–55, http://dx.doi.org/10.1007/s00410-001-0330-9

——— 2003, Fluid infiltration and transport of major, minor, and trace elements during regional metamorphism of carbonate rocks, Wepawaug Schist, Connecticut, USA: American Journal of Science, v. 303, n. 9, p. 753–816, http://dx.doi.org/10.2475/ajs.303.9.753

——— 2005, Deep Crustal Metamorphism of South-Central Connecticut, *in* McHone, N. W., and Peterson, M. J., editors, Guidebook to field trips in Connecticut: New Haven, Connecticut, Yale University, New England Intercollegiate Geological Conference, 97th Annual Meeting, p. 107–119.

Alexander, E. C. J., Michelson, G. M., and Lanphere, M. A., 1978, MMhb-1: A new ^{40}Ar-^{39}Ar dating standard, *in* Zartman, R. E., editor, Short papers for the Fourth International Conference, Geochronology, Cosmochronology, Isotope Geology: Open-File report 78-701, US Geological Survey, p. 6–8.

Armstrong, T. R., Walsh, G. J., and Spear, F. S., 1997, A transect across the Connecticut Valley sequence in eastcentral Vermont, Trip A6, *in* Grover, T. W., Mango, H. N., and Hasenohr, E. J., editors, Guidebook to field trips in Vermont and adjacent New Hampshire and New York: Castelton, Vermont, Castelton State College, New England Intercollegiate Geological Conference, 89th Annual Meeting, p. A6-1–A6-6.

Bell, T. H., and Newman, R., 2006, Appalachian orogenesis: The role of repeated gravitational collapse, *in* Mazzoli, S., and Butler, R. W. H., editors, Styles of Continental Contraction: Geological Society of America Special Papers, v. 414, p. 95–118, http://dx.doi.org/10.1130/2006.2414(06)

Boronkay, K., and Doutsos, T., 1994, Transpression and transtension within different structural levels in the central Aegean region: Journal of Structural Geology, v. 16, n. 11, p. 1555–1573, http://dx.doi.org/10.1016/0191-8141(94)90033-7

Clark, G. S., and Kulp, J. L., 1968, Isotopic age study of metamorphism and intrusion in western Connecticut and southeastern New York: American Journal of Science, v. 266, n. 10, p. 865–894, http://dx.doi.org/10.2475/ajs.266.10.865

Crittenden, M. D., 1980, Metamorphic core complexes of the North America Cordillera; summary, *in* Crittenden, M. D., Coney, J. P., and Davis, G. H., editors, Cordilleran Metamorphic Core Complexes: Geological Society of America Memoirs, v. 153, p. 485–490, http://dx.doi.org/10.1130/MEM153-p485

Currie, K. L., van Staal, C. R., Peter, J. M., and Rogers., N., 2003, Conditions of metamorphism of the main massive sulfide deposits and surrounding rocks in the Bathurst mining camp *in* Goodfellow, W. D., McCutcheon, S. R., and Peter, J. M., editors, Massive sulfide deposits of the Bathurst mining camp, New Brunswick and northern Maine: Economic Geology Monograph 11, p. 65–78.

Dalrymple, G. B., Alexander, E. C. J., Lanphere, M. A., and Kracker, G. P., 1981, Irradiation of samples for $^{40}Ar/^{39}Ar$ dating using the Geological Survey TRIGA reactor: U.S. Geological Survey Professional Paper 1176, 55 p.

Dietsch, C., Kunk, M., Aleinikoff, J., and Sutter, J., 2010, The tectono-thermal evolution of the Waterbury dome, western Connecticut, based on U-Pb and $^{40}Ar/^{39}Ar$ ages: Geological Society of America Memoirs, v. 206, p. 141–181, http://dx.doi.org/10.1130/2010.1206(08)

Dymek, R. F., 1983, Titanium, aluminum and interlayer cation substitutions in biotite from high-grade gneisses, West Greenland: American Mineralogist, v. 68, n. 9–10, p. 880–899.

Fleck, R. J., Sutter, J. F., and Elliot, D. H., 1977, Interpretation of discordant $^{40}Ar/^{39}Ar$ age spectra of Mesozoic tholeiites from Antarctica: Geochimica et Cosmochimica Acta, v. 41, n. 1, p. 15–32, http://dx.doi.org/10.1016/0016-7037(77)90184-3

Fritts, C. E., 1962, Bedrock geology of the Mount Carmel and Southington quadrangles, Connecticut: United States Geological Survey Open-File Report 62–48, p. 161.

——— 1965a, Bedrock geologic map of the Ansonia Quadrangle, Fairfield and New Haven counties, Connecticut: United States Geological Survey Geologic Quadrangle Map Report: GQ-0426, scale 1:24000.

——— 1965b, Bedrock Geologic Map of the Milford Quadrangle, Fairfield and New Haven Counties, Connecticut: United States Geological Survey Geologic Quadrangle Map Report: GQ-0427, scale 1:24000.

Gerbi, C., and West, D. P., 2007, Use of U-Pb geochronology to identify successive, spatially overlapping tectonic episodes during Silurian-Devonian orogenesis in south-central Maine, USA: Geological Society of America Bulletin, v. 119, n. 9–10, p. 1218–1231, http://dx.doi.org/10.1130/B26162.1

Goldsmith, R., Ratcliffe, N. M., Robinson, P., and Stanley, R. S., 1983, Bedrock Geologic Map of Massachusetts: U.S. Geological Survey 3 sheets, scale 1:250,000.

Gray, D. R., 1977, Morphologic classification of crenulation cleavage: Journal of Geology, v. 85, n. 2, p. 229–235, http://dx.doi.org/10.1086/628287

Growdon, M. L., Proctor, B. P., and Wintsch, R. P., 2006, Acadian dextral transpression and strain partitioning along the southeastern margin of the Pumpkin Ground gneiss, Connecticut, USA: Geological Society of America Abstracts with Programs, v. 38.

Hatcher, R. D., 2005, North America; Southern and Central Appalachians, *in* Selley, R. C., Cocks, L. R. M., and Plimer, I. R., editors, Encyclopedia of Geology—Reference Module in Earth Systems and Environmental Sciences: Oxford, Elsevier Academic Press, p. 72–81, http://dx.doi.org/10.1016/B0-12-369396-9/00408-1

Haugerud, R. A., and Kunk, M. J., 1988, ArAr*, a computer program for reduction of $^{40}Ar/^{39}Ar$: U.S. Geological Survey Open-File Report, v. 88–261, 68 p.

Heritsch, F., 1912, Fortschritte in der Kenntnis des geologischen Baues der Zentralalpen öestlich vom Brenner. I. Die Hohen Tauern: Geologische Rundschau, v. 3, n. 3, p. 172–194, http://dx.doi.org/10.1007/BF01801987

Hibbard, J. P., van Staal, C. R., Rankin, D. W., and Williams, H., 2006, Lithotectonic map of the Appalachian Orogen, Canada-United States of America: Geological Survey of Canada Map 2096A, scale 1:1500000.

Hoffman, P. F., 1988, United plates of America, the birth of a craton: Early Proterozoic assembly and growth of Laurentia: Annual Reviews of Earth and Planetary Science, v. 16, p. 543–603, http://dx.doi.org/10.1146/annurev.ea.16.050188.002551

Hsu, K. J., 1955, Monometamorphism, polymetamorphism and retrograde metamorphism: American Journal of Science, v. 253, n. 4, p. 237–239, http://dx.doi.org/10.2475/ajs.253.4.237

Jacobson, C. E., 1997, Metamorphic convergence of the upper and lower plates of the Vincent thrust, San Gabriel Mountains, southern California, USA: Journal of Metamorphic Geology, v. 15, n. 1, p. 155–165, http://dx.doi.org/10.1111/j.1525-1314.1997.00009.x

Jäger, E., 1979, The Rb-Sr method, *in* Jäger, E., and Hunziker, J. C., editors, Lectures in isotope geology: New York, Springer, p. 13–26.

Kunk, M. J., Wintsch, R. P., Naeser, C. W., Naeser, N. D., Southworth, C. S., Drake, A. A., and Becker, J. L., 2005, Contrasting tectonothermal domains and faulting in the Potomac terrane, Virginia-Maryland-discrimination by Ar-40/Ar-39 and fission-track thermochronology: Geological Society of America Bulletin, v. 117, n. 9–10, p. 1347–1366, http://dx.doi.org/10.1130/B25599.1

Lancaster, P. J., Baxter, E. F., Ague, J. J., Breeding, C. M., and Owens, T. L., 2008, Synchronous peak Barrovian metamorphism driven by syn-orogenic magmatism and fluid flow in southern Connecticut, USA: Journal of Metamorphic Geology, v. 26, n. 5, p. 527–538, http://dx.doi.org/10.1111/j.1525-1314.2008.00773.x

Lanzirotti, A., and Hanson, G. N., 1995, U-Pb dating of major and accessory minerals formed during metamorphism and deformation of metapelites: Geochemica et Cosmochimica Acta, v. 59, n. 12, p. 2513–2526, http://dx.doi.org/10.1016/0016-7037(95)00146-8

——— 1996, Geochronology and geochemistry of multiple generations of monazite from the Wepawaug

Schist, Connecticut, USA: implications for monazite stability in metamorphic rocks: Contributions to Mineralogy and Petrology, v. 125, n. 4, p. 322–340, http://dx.doi.org/10.1007/s004100050226

Matthews, J. A., and Wintsch, R. P., 2008, Integrating thermochronology with thermobarometry to resolve a contradictory metamorphic gradient: Abstracts with Programs—Geological Society of America, v. 40, p. 205–205.

McDougall, I., and Harrison, T. M., 1999, Geochronology and thermochronology by the $^{40}Ar/^{39}Ar$ Method: New York, Oxford University Press, 269 p.

McWilliams, C., ms, 2008, The tectonic evolution of the Connecticut Valley synclinorium: contraints from $^{40}Ar/^{39}Ar$ thermochronology, uranium-lead geochronology, thermobarometry and thermal modeling: Bloomington, Indiana, Indiana University, Ph. D. thesis, 199 p.

McWilliams, C. K., Wintsch, R. P., and Kunk, M. J., 2005, Devonian and Carboniferous ages of multiple cleavages in the Waits River Formation, East Athens Dome area, Vermont: Geological Society of America Abstracts with Programs, v. 37, p. 77.

——— 2007, Scales of equilibrium and disequilibrium during cleavage formation in chlorite and biotite-grade phyllites, SE Vermont: Journal of Metamorphic Geology, v. 25, n. 8, p. 895–913, http://dx.doi.org/10.1111/j.1525-1314.2007.00734.x

McWilliams, C. K., Kunk, M. J., Wintsch, R. P., and Bish, D. L., 2013, Determining Ages of Multiple Muscovite-Bearing Foliations in Phyllonites Using the $^{40}Ar/^{39}Ar$ Step Heating Method: Applications to the Alleghanian Orogeny in Central New England: American Journal of Science, v. 313, n. 10, p. 996–1016, http://dx.doi.org/10.2475/10.2013.02.

Moecher, D. P., Cosca, M. A., and Hanson, G. N., 1997, Petrologic and $^{40}Ar/^{39}Ar$ geochronological constrains on the middle to late Paleozoic thermotectonic history of the southern Connecticut Valley zone, New England Appalachians: Geological Society of America Bulletin, v. 109, n. 2, p. 164–175, http://dx.doi.org/10.1130/0016-7606(1997)109⟨0164:PAAAGC⟩2.3.CO;2

Mukherjee, S., and Koyi, H. A., 2010, Higher Himalayan Shear Zone, Sutlej section: structural geology and extrusion mechanism by various combinations of simple shear, pure shear and channel flow in shifting modes: International Journal of Earth Sciences, v. 99, n. 6, p. 1267–1303, http://dx.doi.org/10.1007/s00531-009-0459-8

Oliver, N., 1996, Review and classification of structural controls on fluid flow during regional metamorphism: Journal of Metamorphic Geology, v. 14, p. 477–492, http://dx.doi.org/10.1046/j.1525-1314.1996.00347.x

Olivier, P., Gleizes, G., and Paquette, J. L., 2004, Gneiss domes and granite emplacement in an obliquely convergent regiome; new interpretation of the Variscan Agly Massif; eastern Pyrenees, France *in* Whitney, D. L., Teyssier, C., and Siddoway, C. S., editors, Gneiss Domes in Orogeny: Geological Society of America Special Papers, v. 380, p. 229–242, http://dx.doi.org/10.1130/0-8137-2380-9.229

Passchier, C. W., 1984, Mylonite-dominated footwall geometry in a shear zone, central Pyrenees: Geological Magazine, v. 121, n. 5, p. 429–436,http://dx.doi.org/10.1017/S0016756800029964

Pe-Piper, G., and Piper, D. J. W., 2004, The effects of strike-slip motion along the Cobequid-Chedabucto-southwest Grand Banks fault system on the Cretaceous-Tertiary evolution of Altantic Canada: Canadian Journal of Earth Science, v. 41, n. 7, p. 799–808, http://dx.doi.org/10.1139/e04-022

Phillips, E. R., and Auton, C. A., 1997, Ductile fault rocks and metamorphic zonation in the Dalradian of the Highland Border SW of Stonehaven, Kincardineshire: Scottish Journal of Geology, v. 33, p. 83–93, http://dx.doi.org/10.1144/sjg33010083

Rankin, D. W., 1976, Appalachian salients and recesses: late Precambrian continental breakup and the opening of the Iapetus Ocean: Journal of Geophysical Research, v. 81, n. 32, p. 5605–5619, http://dx.doi.org/10.1029/JB081i032p05605

Ratcliffe, N. M., 1994, Stratigraphic notes, 2, the Wilcox Formation of Vermont Assigned to the Mount Holly Complex: U.S. Geological Survey Bulletin, v. 2060, p. 11–18.

Ratcliffe, N. M., and Bahrami, B., 1976, Chatham fault: A reinterpretation of the contact relationships between the Giddings Brook and Chatham slices of the Taconic allochthon in New York: Geology, v. 4, n. 1, p. 56, http://dx.doi.org/10.1130/0091-7613(1976)4⟨56:CFAROT⟩2.0.CO;2

Ratcliffe, N. M., Stanley, R. S., Gale, M. H., Thompson, P. J., Walsh, G. J., Hatch, J., Norman L., Rankin, D. W., Doolan, B. L., Kim, J., Mehrtens, C. J., Aleinikoff, J. N., McHone, J. G., and Masonic, L. M., 2011, Bedrock geologic map of Vermont: United States Geological Survey 3 sheets, scale 1:100000.

Roden-Tice, M. K., and Wintsch, R. P., 2002, Early Cretaceous normal faulting in southern New England: evidence from apatite and zircon fission-track ages: The Journal of Geology, v. 110, n. 2, p. 159–178, http://dx.doi.org/10.1086/338281

Rodgers, J., 1970, The Tectonics of the Appalachians: New York, Wiley-Interscience, 272 p.

——— 1985, Bedrock Geological Map of Connecticut: State of Connecticut Natural Resources Center, Department of Environmental Protection, scale 1:25,000.

St. Peter, C., 1993, Maritimes Basin evolution: key geologic and seismic evidence from the Moncton Subbasin of New Brunswick: Atlantic Geology, v. 29, n. 3. p. 233–270.

Sevigny, J. H., and Hanson, G. N., 1993, Orogenic evolution of the New England Appalachians of southwestern Connecticut: Geological Society of America Bulletin, v. 105, n. 12, p. 1591–1605, http://dx.doi.org/10.1130/0016-7606(1993)105⟨1591:OEOTNE⟩2.3.CO;2

Shea, W. T., Jr., and Kronenberg, A. K., 1993, Strength and anisotropy of foliated rocks with varied mica contents: Journal of Structural Geology, v. 15, n. 9–10, p. 1097–1121, http://dx.doi.org/10.1016/0191-8141(93)90158-7

Simancas, J. F., Tahiri, A., Azor, A., and Lodeiro, F. J., Poyatos, D. J. M., and Hadi, H. E., 2005, The tectonic frame of the Variscan–Alleghanian orogen in Southern Europe and Northern Africa: Tectonophysics, v. 398, n. 3–4, p. 181–198, http://dx.doi.org/10.1016/j.tecto.2005.02.006

Steiger, R. H., and Jäger, E., 1977, Subcommission on geochronology: Convention on the use of decay constants in geo- and cosmochronology: Earth and Planetary Science Letters, v. 36, n. 3, p. 359–362, http://dx.doi.org/10.1016/0012-821X(77)90060-7

Streule, M. J., Searle, M. P., Waters, D. J., and Horstwood, M. S. A., 2010, Metamorphism, melting, and channel flow in the Greater Himalayan Sequence and Makalu leucogranite: Constraints from thermobarometry, metamorphic modeling, and U-Pb geochronology: Tectonics, v. 29, n. 5, p. 1–28, http://dx.doi.org/10.1029/2009TC002533

Sturt, B. A., Pringle, L. R., and Ramsay, D. M., 1978, The Finnmarkian phase of the Caledonian Orogeny: Journal of the Geological Society, London, v. 135, n. 6, p. 597–610, http://dx.doi.org/10.1144/gsjgs.135.6.0597

Swanson, M. T., 1992, Late Acadian–Alleghenian transpressional deformation: evidence from asymmetric boudinage in the Casco Bay area, coastal Maine: Journal of Structural Geology, v. 14, n. 3, p. 323–341, http://dx.doi.org/10.1016/0191-8141(92)90090-J

Thomas, W. A., 2006, Tectonic inheritance at a continental margin: GSA Today, v. 16, n. 2, p. 4–11, http://dx.doi.org/10.1130/1052-5173(2006)016[4:TIAACM]2.0.CO;2

Waldron, J. W. F., Roselli, C. G., Utting, J., and Johnston, S. K., 2010, Kennetcook thrust system: late Paleozoic transpression near the southern margin of the Maritimes Basin, Nova Scotia: Canadian Journal of Earth Science, v. 47, n. 2, p. 137–159, http://dx.doi.org/10.1139/E09-071

Walsh, G. J., Valley, P. M., and Sicard, K. R., 2012, A transect through the base of the Bronson Hill anticlinorium in western New Hampshire, *in* Thompson, P. J., and Thompson, T. B., editors, Guidebook to field trips in western New Hampshire and adjacent Vermont and Massachusetts: Newbury, New Hampshire, Keene State College, New England Intercollegiate Geological Conference, 104th Annual Meeting Mount Sunapee Resort, p. 83–103.

Wang, C., Ludman, A., and Xiao, L., 2006, A Transect across the Norumbega Fault System and Fault-controlled Post-Acadian Redbeds and Post-redbed Turner Mountain Syenite, East of Old Town, *in* Gibson, D., Daly, J., and Reusch, D., editors, Guidebook to field trips in Maine: Orono, Maine, University of Maine, New England Intercollegiate Geological Conference, 98th Annual Meeting, p. 57–75.

Wilson, J. T., 1966, Did the Atlantic close and then re-open?: Nature (London), v. 211, p. 676–681, http://dx.doi.org/10.1038/211676a0

Wintsch, R., Kunk, M. J., Mulvey, B. K., and Southworth, C. S., 2010, $^{40}Ar/^{39}Ar$ dating of Silurian and Late Devonian cleavages in lower greenschist-facies rocks in the Westminster terrane, Maryland, USA: Geological Society of America Bulletin, v. 122, n. 5–6, p. 658–677, http://dx.doi.org/10.1130/B30030.1

Wintsch, R. P., Sutter, J. F., Kunk, M. J., Aleinikoff, J. M., and Dorais, M. J., 1992, Contrasting P-T-t paths: thermochronologic evidence for a late Paleozoic final assembly of the Avalon composite terrane in the New England Appalachians: Tectonics, v. 11, n. 3, p. 672–689, http://dx.doi.org/10.1029/91TC02904

Wintsch, R. P., Kunk, M. J., Boyd, J. L., and Aleinikoff, J. N., 2003, P-T-t paths and differential Alleghanian loading and uplift of the Bronson Hill terrane, south central New England: American Journal of Science, v. 303, n. 5, p. 410–466, http://dx.doi.org/10.2475/ajs.303.5.410

York, D., 1969, Least squares fitting of a straight line with correlated errors: Earth and Planetary Science Letters, v. 5, p. 320–324, http://dx.doi.org/10.1016/S0012-821X(68)80059-7